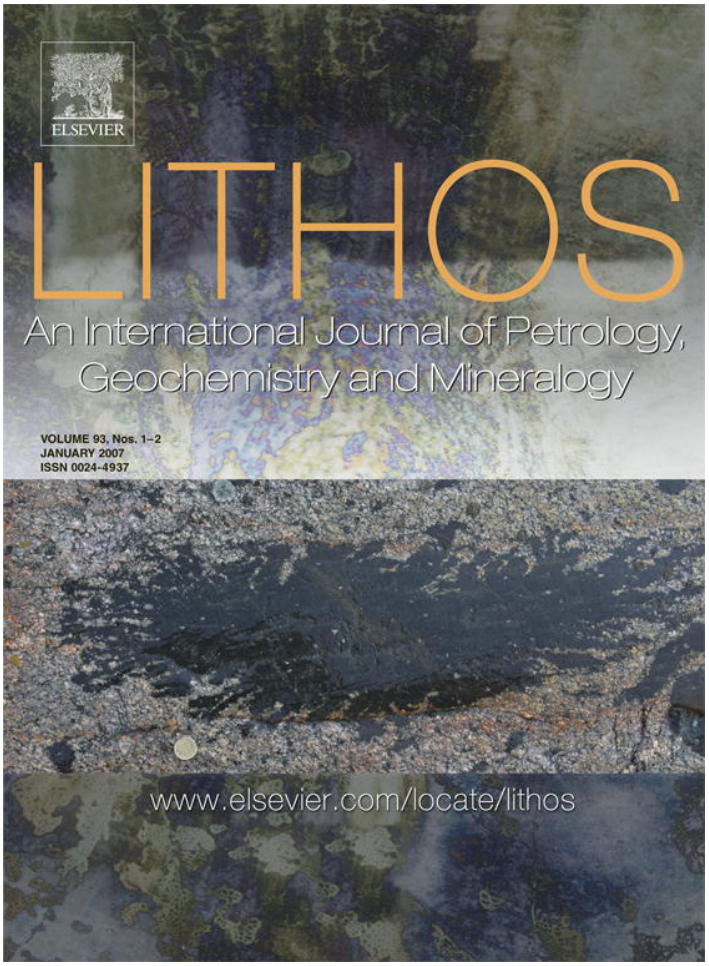
Provided for non-commercial research and educational use only.
Not for reproduction or distribution or commercial use.



This article was originally published in a journal published by Elsevier, and the attached copy is provided by Elsevier for the author's benefit and for the benefit of the author's institution, for non-commercial research and educational use including without limitation use in instruction at your institution, sending it to specific colleagues that you know, and providing a copy to your institution's administrator.

All other uses, reproduction and distribution, including without limitation commercial reprints, selling or licensing copies or access, or posting on open internet sites, your personal or institution's website or repository, are prohibited. For exceptions, permission may be sought for such use through Elsevier's permissions site at:

http://www.elsevier.com/locate/permissionusematerial

Available online at www.sciencedirect.com
ScienceDirect
Lithos 93 (2007) 126–148
LITHOS
www.elsevier.com/locate/lithos

Metasomatic silicate chemistry at the Bayan Obo Fe–REE–Nb deposit, Inner Mongolia, China: Contrasting chemistry and evolution of fenitising and mineralising fluids

M.P. Smith *

School of the Environment, University of Brighton, Cockcroft Building, Lewes Road, Brighton, BN2 4GJ, United Kingdom
Department of Mineralogy, The Natural History Museum, Cromwell Road, London, SW7 5BD, United Kingdom

Received 11 October 2005; accepted 29 June 2006
Available online 8 August 2006

Abstract

Fenite aureoles around carbonatite dykes, and alteration associated with Fe–REE–Nb ore bodies at Bayan Obo, Inner Mongolia, China, show alkali silicate assemblages containing aegirine–augite, (magnesio-)riebeckite, (magnesio-)arfvedsonite, and phlogopite, accompanied by varying amounts of apatite, albite and quartz. In both fenites and orebodies simple thermodynamic constraints indicate mineral parageneses are consistent with rock buffered cooling accompanied by the infiltration of a range of externally buffered hydrothermal fluids. Statistical analysis of amphibole chemistry indicates that even in apparently texturally well constrained paragenetic stages wide variations in chemistry occur in both the ore bodies and fenites. Much of this variation is attributable to the Mg and F content of amphibole, and is therefore interpreted as a result of variation in externally controlled variables (*P*, *T*, initial fluid composition) rather than internally controlled variables such as protolith composition. Similarities in chemistry exist between fenite and some ore body amphiboles. Thermodynamic analysis of the composition of biotite and apatite allows constraints to be placed on the F-content of hydrothermal fluids, and indicates relatively consistent compositions in fenites and orebodies ($\log a_{HF}/a_{H_2O} = -3.8$ to -3.6 at 300 °C and 1 kbar). Amphibole and biotite associated with niobate mineralization are both enriched in fluorine relative to the rest of the paragenesis, and biotite compositions indicate significantly higher HF activities in the hydrothermal fluid ($\log a_{HF}/a_{H_2O} = -2.6$ at 300 °C and 1 kbar). The data presented here reinforce previous interpretations of the complex, multistage nature of mineralisation at Bayan Obo, but are still consistent with a direct involvement of carbonatite derived fluids during ore genesis.
© 2006 Elsevier B.V. All rights reserved.

Keywords: Amphibole; Biotite; Fenite; Bayan Obo; Fluid chemistry

1. Introduction

The Fe–REE–Nb deposit at Bayan Obo, Inner Mongolia, China, is the world's largest known rare-earth element (REE) resource, and formed by multiple episodes of hydrothermal activity (Drew et al., 1990; Yuan et al., 1992; Chao et al., 1992, 1993, 1997). Much interest has been focused on the deposit because of its extraordinary metal concentrations, and its similarities to both carbonatitic deposits and the broad group of igneous-related Fe-oxide–(Cu–U–Au–REE) deposits (Hitzman et al., 1992). Various origins have been proposed (reviewed by Wu et al., 1996; Smith and Wu, 2000), with models involving fluids derived

* School of the Environment, University of Brighton, Cockcroft Building, Lewes Road, Brighton, BN2 4GJ, United Kingdom. Tel.: +44 1273 642265; fax: +44 1273 642285.
E-mail address: martin.smith@brighton.ac.uk.

0024-4937/$ - see front matter © 2006 Elsevier B.V. All rights reserved.
doi:10.1016/j.lithos.2006.06.013

Author's personal copy

from carbonatite or alkaline magmatism (Drew et al., 1990; Yuan et al., 1992; Campbell and Henderson, 1997), subduction (Chao et al., 1992, 1997; Wang et al., 1994), or A-type granite magmatism (Chao et al., 1997). Unequivocal carbonatites do occur in the Bayan Obo area, but no previous attempts have been made to compare the associated fenitisation with the alteration within and surrounding the ore bodies.

This paper presents new textural descriptions and analyses of alteration phases from both fenites and ore bodies, carried out in order to examine links between the carbonatite dykes and the hydrothermal alteration within the orebodies. These data are examined in terms of their implications for fluid compositions. Using an internally consistent thermodynamic database allows fluid compositions to be calculated in terms of species activities, which can then be more easily related to fluid compositions (Zhu and Sverjensky, 1991), than halogen acid fugacities (e.g. Munoz, 1984). New data from Bayan Obo are important in the further development of models for ore genesis in the area, and are relevant to problems relating to the hydrothermal mobility of the high field strength elements (HFSE), particularly the REE and niobium, and understanding the processes involved in alkaline alteration.

2. Geological setting

The Bayan Obo Fe–REE–Nb deposit is located in Inner Mongolia, China (109° 59′ E; 41° 48′ N), and has estimated total reserves of 600 Mt of iron oxides (Yuan et al., 1992) and in excess of 100 Mt REE–oxide (Ren, 1985). The deposit is contained within the sediments of the Proterozoic Bayan Obo Group (Fig. 1), which consists

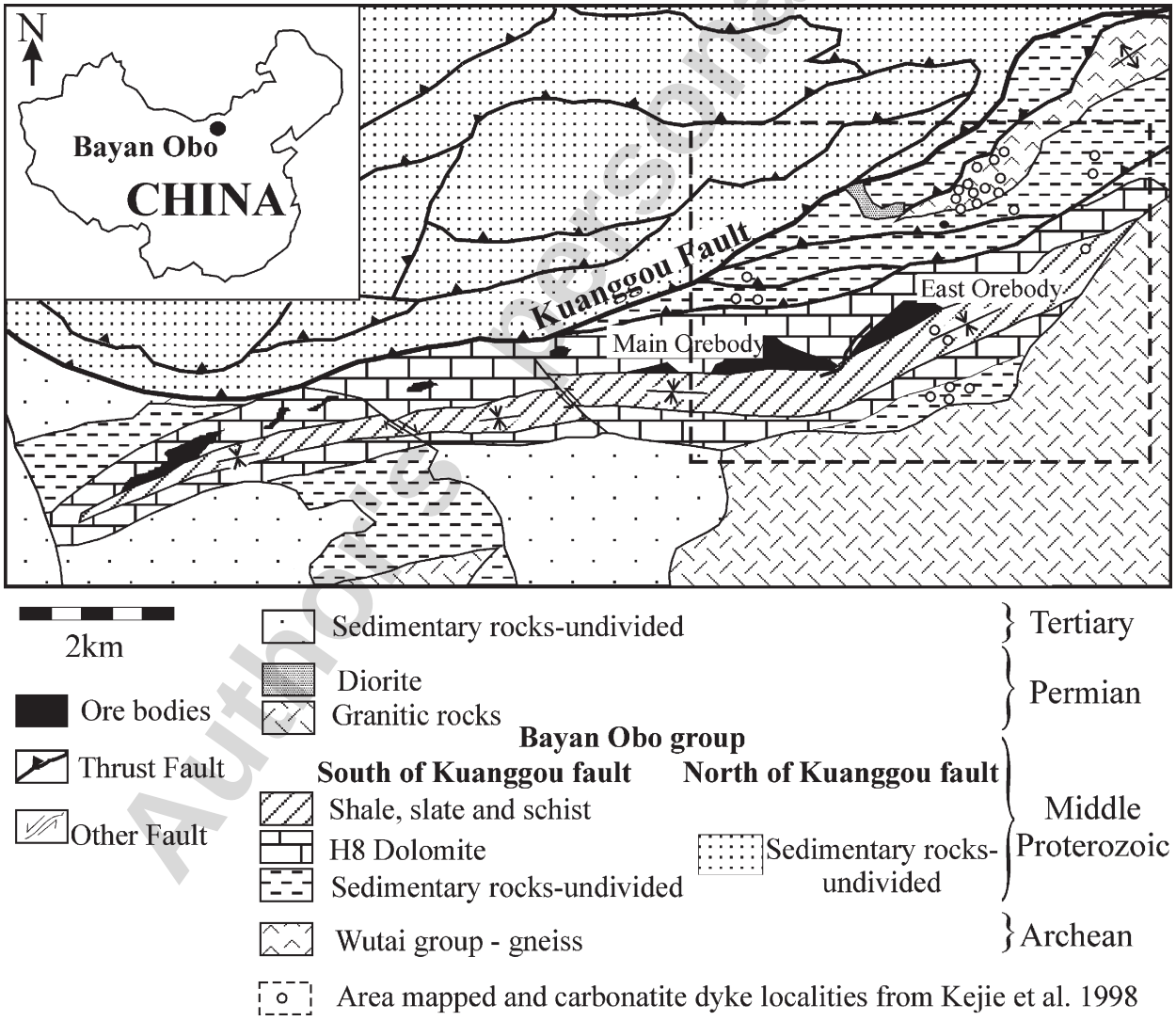


Fig. 1. Sketch map of the geology surrounding the Bayan Obo ore deposits, adapted from Chao et al. (1992). Also shown are the area mapped and locations of carbonatite dykes from Tao et al. (1998).

Author's personal copy

Table 1
Localities and brief descriptions of samples used in this study

Sample number	Location [a]		Description
Carbonatites and fenites			
1995 P3(30)	41°48.234′ N 109°59.100′ E	Base level East Ore body pit	Albitite vein/dyke + fenite
1999 P7(96)	41° 45′ N 110°E	North of main pit	Fenitised Quartzite, Wu carbonatite
1999 P7(103)	41° 45′ N 110°E	North of main pit	Aegirine–riebeckite fenite–Wu carbonatite
1999 P7(117)	41° 45′ N 110°E	North of main pit	Carbonatite and fenite–Dulahala carbonatite
1999 P7(118)	41° 45′ N 110°E	North of main pit	Western margin Dulahala carbonatite
Banded ores			
1996 P4(11)	41°48′ N 109°59′ E	E. pit, 1582 m level	Huanghoite bearing banded ore
1995 P3(16)	41°47.891′ N 109°58.129′ E	Main pit, 1626 m level	Coarse amphibole in banded ore
1996 P4(12)	41°48′ N 109°59′ E	E. pit, N-side, 1582 m level	Massive magnetite–aegirine–fluorite rock
1996 P4 (17)	41°47′ N 109°58′ E	Main pit	Banded ore
1996 P4 (6)	41°48′ N 109°59′ E	E. pit, N-side	Banded ore with later veins of fluorite.
1995 P3 (29)	41°48.234′ N 109°59.100′ E	E. pit, N-side, 1558 m level	Biotite-bearing banded ore
1995 P3 (17)	41°47.891′ N 109°58.129′ E	Main pit, N-side, 1626 m level	Fluoritized, banded H8. Magnetite-rich. Coarse, relatively unbanded
1995 P3 (13)	41°47.891′ N 109°58.129′ E	Main pit, N-side, 1626 m level	Magnetite–fluorite rock from H8
Banded ore veins			
1996 P4(18)	41°47′ N 109°58′ E	Main pit	Fluorite vein
1996 P4(25)	41°48′ N 109°59′ E	E.pit, 1582 m level	Aegirine–apatite vein
1996 P4 (46)	41°48′ N 109°59′ E	E. pit, 1558 m level	Fluoritized, banded H8 dolomite with lenses of apatite, cut by aegirine vein
1995 P3(7)	41°48.722′ N 109°58.340′ E	Main pit, N-side, 1626 m level	Aegirine vein cutting aegirine rock
1995 P3(18)	41°47.891′ N 109°58.129′ E	Main pit, N-side, 1626 m level	Aegirine vein cutting aegirine rock
Partially altered dolomite			
1996 P4(52)	41°48′ N 109°59′ E	E. pit, 1650 m level	Amphibole bearing marble
1996 P4 (7)	41°48′ N 109°59′ E	E.pit	Altered dolomite
Altered siliclastics			
1999 P7(127)	41° 45′ N 110°E.	E. pit, base level	Contact dolomite–siliciclastics
1999 P7(40)	41° 45′ N 110°E.	W. end, E. pit	Slate
Niobate associated			
1999 P7 (68)	41° 45′ N 110°E.	Top level, main pit	Aeschynite–riebeckite vein
1999 P7(67)	41° 45′ N 110°E.	Top level, main pit	Aeschynite in banded ore
1996 P4(16)	41°47′ N 109°58′ E	Main pit	Aegirine–aeschynite rock
Permian Skarn			
1999 P7(82)	41° 45′ N 110°E.	East of main pit	Biotite–diopside skarn

[a] Localities to 3 significant figures refer to samples located using hand held GPS.

predominantly of sandstones and slates, with the exception of the H8 dolomite marble unit which hosts the vast majority of the ore. The origin of the host marble is still disputed, and it has been proposed to be either sedimentary in origin (Meng, 1982; Hou, 1989; Chao et al., 1992), or the result of carbonatite magmatism (Yuan et al., 1992; Le Bas et al., 1992; 1997).

The paragenesis of the deposit is complex with, according to Chao et al. (1992; 1993), at least eleven stages from deposition, through metamorphism and mineralisation, to the intrusion of Hercynian granitoids to the south of the deposit. The main stage of REE-element mineralization has been identified as 430 to 420 Ma on the basis of ^{232}Th–^{208}Pb analyses of monazite and bastnäsite by Wang et al. (1994), with a limited number of older ages in the ranges 555–553 Ma and 474–496 Ma. Three periods of metamorphism and metasomatism have been recognised on the basis of ^{40}Ar–^{39}Ar geochronology using alkali amphiboles (Chao et al., 1997). A Proterozoic episode fixes the minimum age of the host marble, a Caledonian episode probably relates to the main ore forming or remobilisation episode, and a Hercynian episode is related to the intrusion of granitoids to the south of the deposit.

Author's personal copy

Table 2
Summary of previous fluid inclusion data from Bayan Obo (Smith and Henderson, 2000)

	Host mineral	Fluid composition	Temperature (°C)	Pressure (kbar)
Disseminated monazite	Monazite	NaCl–H_2O–CO_2 1–5 wt.% NaCl eq. X_{CO_2} 0.15–0.45	>286–362	>0.8–2.0
Banded ores	Apatite	NaCl–H_2O 7–10 wt.% NaCl eq.	>300–400	>0.9–2.4
	Bastnasite	NaCl–H_2O–CO_2 2–6 wt.% NaCl eq. X_{CO_2} 0.08–0.23	>280–340	>0.9–2.5
Aegirine alteration	Aegirine	NaCl–H_2O 5–16 wt.% NaCl eq.	>360–430	>0.8–1.0
Veins	Apatite/bastnasite	NaCl–H_2O–CO_2 1–7 wt.% NaCl eq. X_{CO_2} 0.18–0.54	250–300	0.8–1.0
	Fluorite	1. NaCl–H_2O–CO_2 1–20 wt.% NaCl eq. X_{CO_2} 0.17–0.84 2. NaCl–H_2O 27–60 wt.% NaCl eq.	220–280	0.8–1.0
Fluorite alteration	Fluorite	NaCl–H_2O 5–32 wt.% NaCl eq.	134–270	>0.1
Barite veins and alteration	Barite	NaCl–H_2O 0.2–6.4 wt.% NaCl eq.	129–216	>0.1

Several possible modes of formation have been proposed for the deposit including syngenetic sedimentary deposition (Meng, 1982), metasomatism associated with granitic magmatism (Wang, 1973), and deposition from exhalative, possibly carbonatite-related, hydrothermal fluids (Yuan et al., 1992). The work of Chao et al. (1992, 1993, 1997) has demonstrated an epigenetic origin for the deposit via multistage hydrothermal metasomatism with fluids derived from either subduction (Chao et al., 1992, 1997; Wang et al., 1994), A-type granite magmatism (Chao et al., 1997), or carbonatite, or alkaline, magmatism (Drew et al., 1990; Campbell and Henderson, 1997). The carbonatite model may be reconciled with geochronological and radiogenic isotope data, which suggest an isotopically enriched source for ore metals, if the deposit was formed by remobilisation or thermal metamorphism of an ancient carbonatite or other alkaline igneous source during Caledonian subduction (Smith and Wu, 2000). Caledonian thermal disturbance of older rocks was also suggested by Liu et al. (2004) on the basis of Re–Os analyses of pyrite. Recent SHRIMP dating of single zircon crystals from within coarse grained dolomite marble in the main H8 unit showed igneous derived zircon cores with Proterozoic ages (1370–1257 Ma), and metamorphic or hydrothermal rims with Caledonian ages (455 +/− 28 Ma; Campbell et al., 2000).

2.1. Carbonatites

At least 28 calcite, dolomite and calcite–dolomite carbonatite dykes have been recognised in the area, ranging from 0.8 to 2.6 m wide (Le Bas et al., 1992; Zhang et al., 1994; Tao et al., 1998). The majority cut the Archean Wu Tai gneiss to the north of the ore bodies,

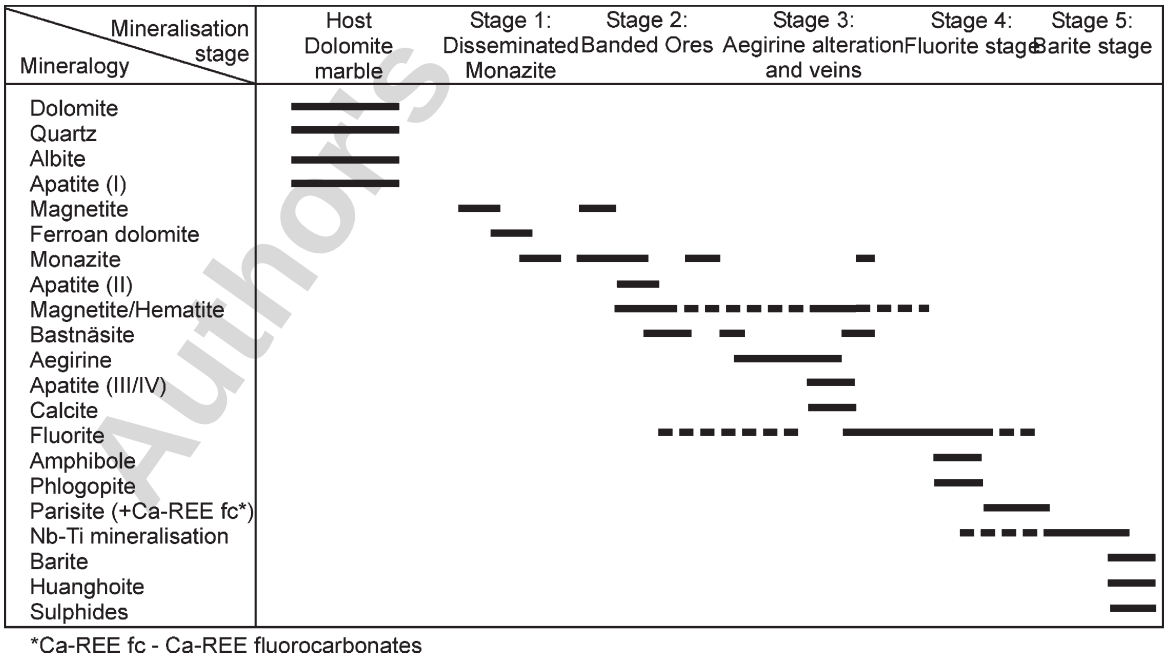


Fig. 2. Simplified summary of the relative paragenesis at Bayan Obo of the main minerals in samples from this study. Parts of the sequence are based on the work of Chao et al. (1992, 1993, 1997). Apatite generations are based on the work of Campbell and Henderson (1997).

Authors personal copy

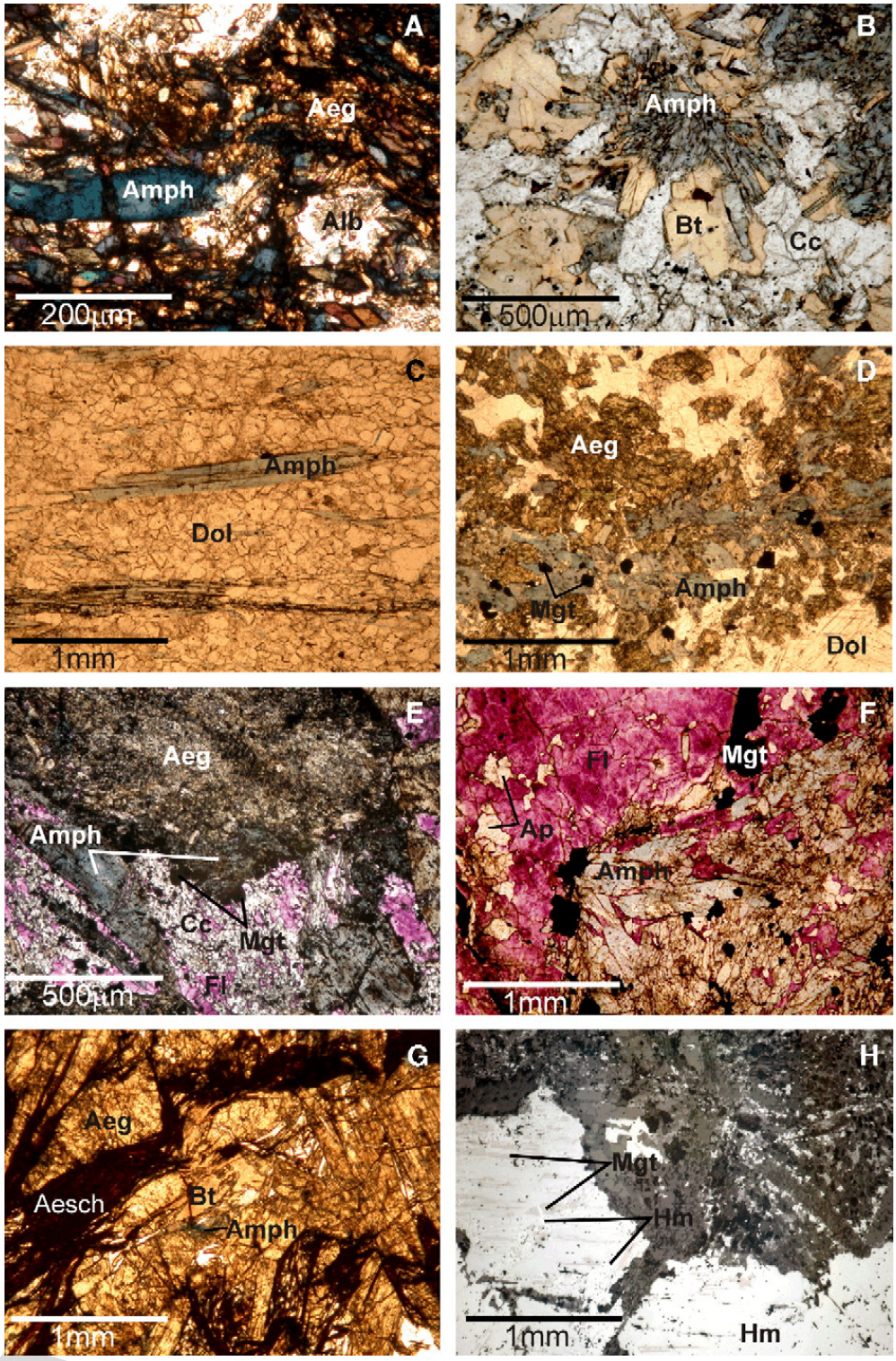


Fig. 3. Photomicrographs of metasomatic textures from carbonatite dykes and ore bodies at Bayan Obo. (A) Aegirine–riebeckite–albite fenite, margins of the Wu carbonatite. Sample 1999, P7(103). (B) Alkali amphibole and biotite in fenite from the albitite dyke, East Ore Body. Sample 1995, P3(30). (C) Acicular amphibole in H8 dolomite marble. Sample 1999, P4(52). (D) Blue amphibole overprinting aegirine and aegirine–augite alteration in banded ore. Sample 1995, P4(7). (E) Amphibole and magnetite replacing the margin of an aegirine grain in fluorite-rich banded ore. Sample 1995, P3(16). (F) Amphibole associated with fluorite–apatite–magnetite vein. Sample 1996, P4(18). (G) Fractured aegirine rock with interstitial aeschynite, amphibole, quartz and biotite. Sample 1996, P4(16). (H) Reflected light photomicrograph of Fe oxides in massive aegirine rock. Two generations of hematite replace magnetite and accompany amphibole alteration of aegirine. Sample 1996, P4(12). Abbreviations: Amph — amphibole; Aeg — aegirine; Alb — albite; Bt — biotite; Cc — calcite; Dol — dolomite; Mgt — magnetite; Hm — hematite; Fl — fluorite; Ap — apatite; Aesch — aeschynite; Qtz — quartz.

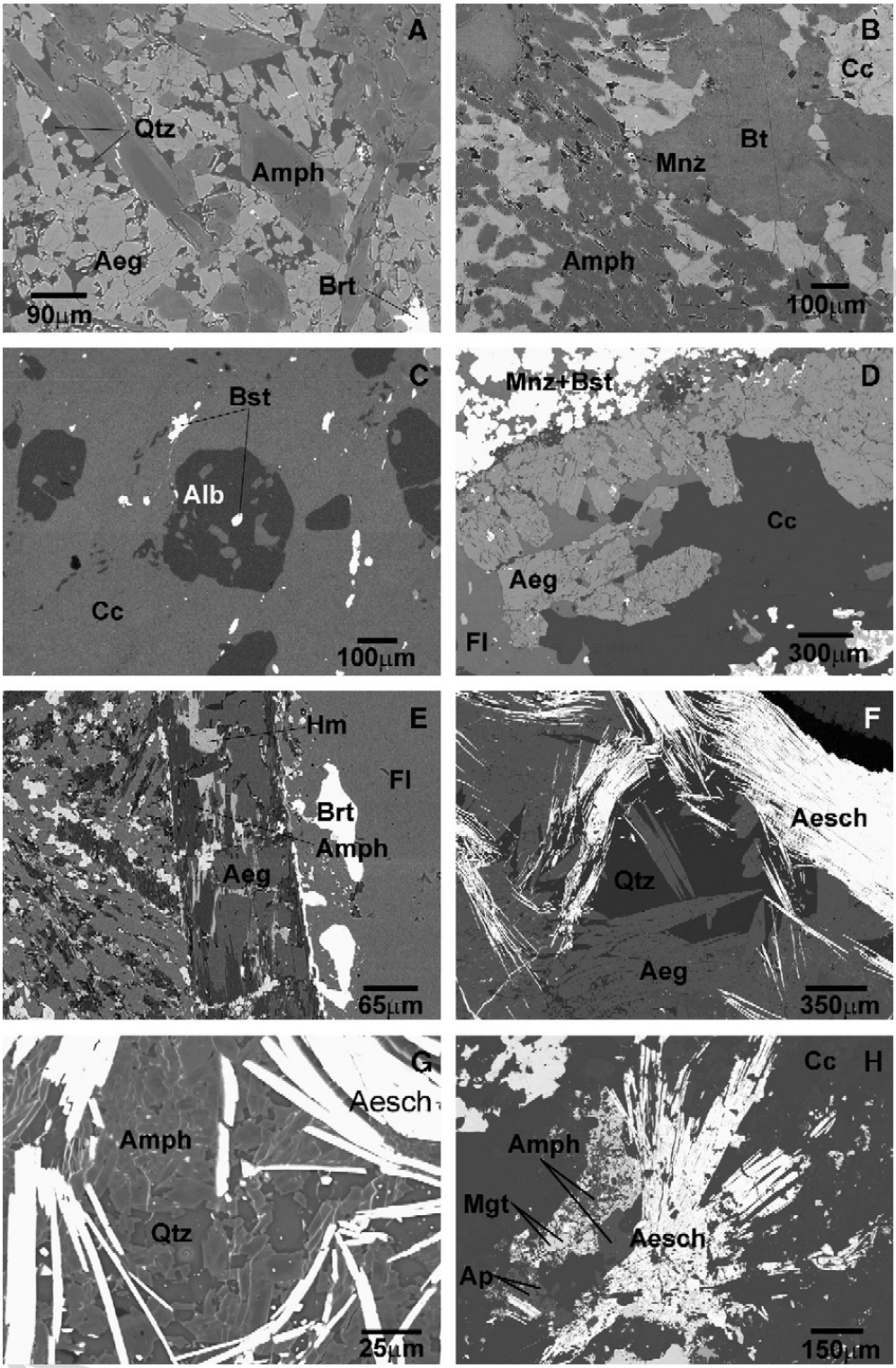


Fig. 4. Backscattered electron (BSE) images of metasomatic textures. (A) Aegirine–riebeckite fenite showing zonation of amphibole, and interstitial quartz and barite, Wu carbonatite. Sample 1999, P7(103). (B) Amphibole–biotite fenite with interstitial calcite, margins of albite dyke. Sample 1995, P3(30). (C) Albite from coarse grained strontian calcite marble. Sample 1996, P4(15). (D) Aegirine–augite associated with monazite–bastnäsite mineralisation in partially altered banded ore. Sample 1996, P4(7). (E) Partial alteration of aegirine to magnetite and amphibole on margins of fluorite–magnetite–barite filled vug space. Sample 1996, P4(12). (F) Aeschynite and quartz filling vug space and fractures in massive aegirine rock. Sample 1996, P4(16). (G) Association of amphibole and quartz with aeschynite in aeschynite–riebeckite vein. Sample 1999, P7(68). (H) Association of aeschynite with amphibole and magnetite, overprinting calcite and apatite in banded ore. Sample 1999, P7(67). Abbreviations as Figure 3, plus: Brt — barite; Mnz — monazite; Bas — basnästite.

but others have been reported from within the Bayan Obo group sediments. They have all been affected by subsequent deformation, and in some cases the dyke margins are intricately folded (Le Bas et al., 1992). The carbonatite dykes have been dated to 1233 +/− 65 Ma (Zhang et al., 1994) and 1208 +/− 12 Ma (Ren et al., 1994) using whole rock Sm–Nd and ^{40}Ar–^{39}Ar techniques respectively. However, Rb–Sr analyses from a single carbonatite dyke gave an age of 433 Ma (Bai and Yuan, 1985), whilst those from a separate fenite sample gave ages of 343 +/− 7 Ma (Zhang et al., 1994). Ren et al. (1994) also obtained a ^{232}Th–^{208}Pb age from carbonatite monazite of 445 +/− 11 Ma. These ages cover a similar range to those from the ore bodies.

3. Methods

The petrography of the samples was first investigated using transmitted light microscopy, and then the back-scattered electron (BSE) mode of a Hitachi S2500 SEM, using a 20 kV accelerating voltage. Mineral analyses were carried out using a Cameca SX50 electron microprobe with an accelerating voltage of 15 kV and a beam current of 20 nA. Individual elements were calibrated against natural and synthetic mineral standards, including halite for Cl, BaF_2 for F, jadeite for Na, KBr for K, wollastonite for Ca and Si, olivine for Mg, celestine for Sr, corundum for Al, rutile for Ti and pure metals for Fe, Mn, Cr and Ni. An empirical correction was made for possible Ti–Ba interferences. Ni and Cr were below detection levels in most samples analysed. Count times were typically 10 s, but were 20 s for the halogens, Mn, Cr and Na. Background count times were half those on the element peak. In silicates F was analysed using a TAP crystal, with backgrounds measured at +1000 and −2010 CU (Cameca Spectrometer Units — 10^5 $\sin^{-1}$ 2θ) relative to the element peak in order to avoid overlaps with second order Kα peaks from Al, Si, Fe and Mg. In apatite it was analysed using a PC1 crystal with backgrounds at +1971 and −1300 to avoid overlap with P peaks. The halogens and alkalis were always analysed first to avoid problems of mobility under the electron beam.

4. Results

4.1. Textural setting of silicate phases

Localities and brief descriptions of the samples used in this study are shown in Table 1, and the results of previous fluid inclusion analyses are summarised in Table 2. The paragenesis is summarised in Fig. 2. In this

Table 3
Representative analyses of pyroxene (aegirine and aegirine–augite) from Bayan Obo

	Carbonatite fenite	Albitite fenite	Banded ores				Banded ore veins		Niobate associated	
	1999, P7 (103)	1995, P3 (30)	1996, P4 (11)	1996, P4 (12)	1996, P4 (17)	1996, P4 (7)	1996, P4 (25)	1995, P3 (18)	1996, P4 (16)	1999, P7 (68)
Na_2O	13.80	12.84	13.63	13.74	13.11	11.79	13.47	12.76	13.02	11.47
K_2O	0.00	0.01	0.01	0.00	0.01	0.00	0.00	0.00	0.01	0.02
CaO	0.42	1.96	0.00	0.18	1.38	3.60	0.28	2.20	1.88	3.57
MgO	0.47	0.88	0.08	0.11	0.65	1.83	0.17	0.79	0.97	1.75
MnO	0.02	0.26	0.01	0.01	0.06	0.25	0.00	0.20	0.20	0.35
Fe_2O_3[a]	31.19	29.47	32.18	33.35	31.95	28.67	33.67	30.87	30.09	28.85
Al_2O_3	1.06	1.24	0.24	0.15	0.54	0.69	0.37	0.85	1.09	0.85
SiO_2	53.26	52.95	52.40	52.49	52.47	52.64	51.89	52.94	52.66	52.21
TiO_2	0.45	0.33	2.00	0.02	0.25	0.29	0.06	0.22	0.16	0.19
Total	100.65	99.92	100.55	100.03	100.41	99.75	99.90	100.83	100.08	99.26
Formulae calculated to 6 O										
Na	1.010	0.945	1.003	1.020	0.967	0.870	1.003	0.935	0.960	0.851
K	0.000	0.000	0.000	0.000	0.000	0.000	0.000	0.000	0.000	0.001
Ca	0.017	0.080	0.000	0.007	0.056	0.147	0.012	0.089	0.077	0.147
Mg	0.027	0.050	0.004	0.006	0.037	0.104	0.010	0.045	0.055	0.101
Mn	0.001	0.008	0.000	0.000	0.002	0.008	0.000	0.006	0.006	0.011
Fe	0.885	0.840	0.918	0.959	0.913	0.819	0.971	0.877	0.859	0.829
Al	0.047	0.055	0.011	0.007	0.024	0.031	0.017	0.038	0.049	0.039
Si	2.014	2.013	1.992	2.013	2.000	2.007	1.996	2.004	2.005	2.001
Ti	0.013	0.009	0.058	0.001	0.007	0.008	0.002	0.006	0.005	0.005

[a] Total Fe calculated as Fe_2O_3.

Author's personal copy

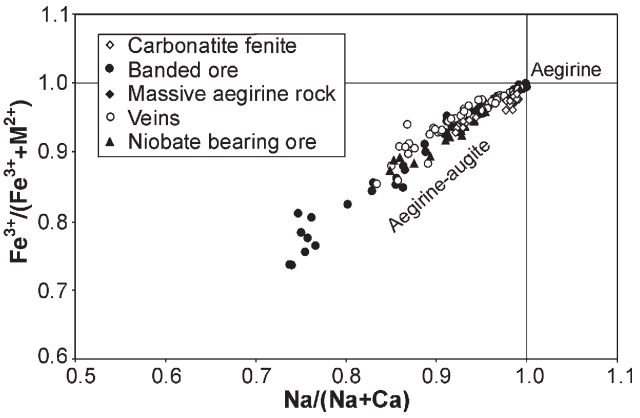


Fig. 5. Pyroxene (aegirine to aegirine–augite) chemistry from Bayan Obo carbonatites and banded ores. M^{2+} refers to Mg+Mn.

study all amphibole samples studied were of prismatic to fibrous amphibole within fenites, the ore-body hosting dolomite or the ore bodies themselves (metasomatic and metasomatic–metamorphic in the terminology of Chao et al., 1997) rather than fibrous to abestiform crystals aligned on foliation planes (metamorphic amphiboles in Chao et al., 1997). Albite, aegirine and aegirine–augite are the paragenetically earliest metasomatic silicate phases, occurring in fenites associated with carbonatite dykes (1999, P7(103)), and the albitite fenite (1995, P3 (30)). In most of these instances they are intimately associated with blue amphibole, and sometimes albite (Figs. 3A and 4A). Blue amphibole also occurs within the margins of the carbonatites (Fig. 3B). In the studied samples biotite only occurs as a fenite phase associated with the albitite dyke (Figs. 3C and 4B). Albite also occurs in the main body of the H8 dolomite marble, associated with manganoan and strontian calcite, and typically showing resorbed edges (Fig. 4C).

Blue amphibole occurs as a relatively common phase in otherwise relatively unaltered dolomite marble (Fig. 3D). Aegirine occurs in massive, unfoliated pods within the banded ore, frequently with open space-filling textures, as bands within the banded ore (Fig. 3E), where in some instances it cuts across the foliation, and in extensional veins which cut the main banded ores at a high angle to the foliation. In the banded ores both amphibole and biotite are paragenetically later than pyroxene, and frequently appear to be associated with fluoritisation. Amphibole replaces earlier aegirine either along the margins of fluorite filled vug space (Fig. 4E) or as clots replacing aegirine within the bands (Fig. 3D, E). More typical banded ore amphibole occurs as coarse-grained (1–5 mm) euhedral crystals, both aligned with or at a significant angle to the foliation, and in some instances bent, or partly boundinaged, parallel to the banding (Fig. 3E). This implies amphibole formation within the banded ores pre- to syn-deformation. Amphibole is also a common vein phase, occurring as a late stage vug space-filling phase in aegirine veins, and as a major component of fluorite–magnetite veins (Fig. 3G). It also occurs infilling vugs within massive aegirine rocks, alongside quartz and niobate minerals including aeschynite ($(REE,Ca,Fe,Th)(Ti,Nb)_2(O,OH)_6$) and pyrochlore (Figs. 3H, I and 4F,G,H). Biotite occurs alongside amphibole in the banded ores, as a late stage phase in aegirine veins, associated with fluoritisation and fluorite veins, and infilling vug space alongside niobium mineralisation (Fig. 3H, I).

Key to understanding the evolution of the silicate paragenesis is the oxygen fugacity during the deposits' evolution. The Bayan Obo deposits show a complex Fe oxide paragenesis, investigated in detail by Chao et al. (1997). Early magnetite was subsequently martised, accompanied by the formation of granular hematite in the banded ores. This is then cut by veins of later stage magnetite. In the samples studied here magnetite is the dominant Fe-oxide typically with incipient hematite alteration along fractures. In the fenite samples studied

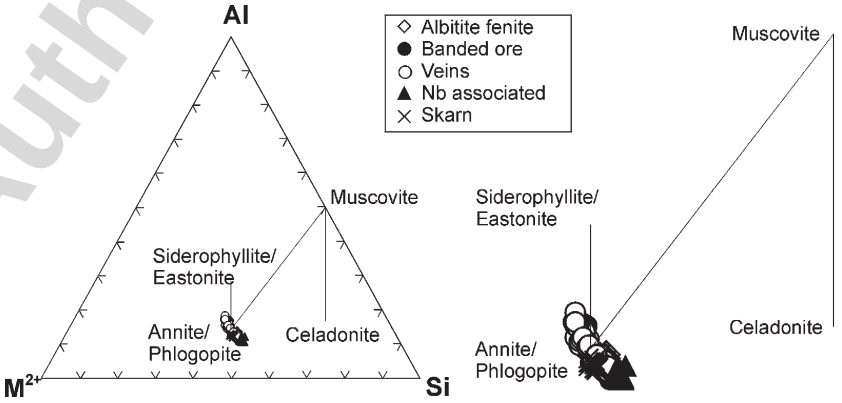


Fig. 6. Ternary diagram in atomic % M^{2+}–Al–Si ($M^{2+}=Fe^{2+}+Mg+Mn$) illustrating the principle substitutions between the dioctahedral and trioctahedral micas (Monier and Robert, 1986), and the composition of Bayan Obo biotites.

Author's personal copy

magnetite is in one instance accompanied by pyrite, but this is probably a late stage overprint associated with the barite stage alteration in the main ore bodies. In the banded ore samples magnetite always has minor hematite developed along cleavage planes, and in sample 1996, P4(12) hematite directly replaces magnetite, with a second generation of hematite developed along fractures (Fig. 3H). Magnetite with minor hematite alteration also dominates the vein samples, except for in barite-bearing examples where pyrite accompanies barite. At the deposit scale, therefore, following the initial mineralisation of the H8 dolomite there was an excess of magnetite which was subsequently partially hematised, providing a buffer for fO_2. The presence of late magnetite veins indicates periodic influxes of unbuffered fluid.

4.2. Aegirine chemistry

All the pyroxene analysed is close to pure aegirine–augite in composition, with a maximum augite mole fraction of around 0.25 (Table 3; Fig. 5). The most Ca-rich aegirines are from the banded ores, where the higher Ca-contents may be a result of the replacement of carbonates. The principle divalent cation substituting on to the octahedral site is Mg, with minor Mn. Contents of Al and Ti are low throughout.

4.3. Biotite chemistry

The results of analyses of biotite chemistry are shown in Figs. 6 and 7 and summarised in Table 4. In all environments the biotites are dominantly phlogopitic (Figs. 6 and 7A) with only minor Fe (atomic ratio Fe/(Fe+Mg) ~0.1 to 0.3). In the albitite fenite, banded ores, niobate-bearing samples and skarn the biotites are typically Al- and M^{2+} depleted and Si-rich relative to ideal biotite mica (Deer et al., 1966). Simple estimates of the amount of Fe^{3+} present, assuming a tetraferriphlogopite component (Brod et al., 2001), indicate negligible Fe^{3+} on the tetrahedral site, but do not rule out the potential presence of Fe^{3+} on octahedral sites. In this case the deficiency in Al can be accounted for by a substitution of the form $(Al^{3+}{}_{-2},M^{2+}{}_{-1}),(Si^{4+}{}_{+2},\square_{+1})$ (Fig. 7B, C).

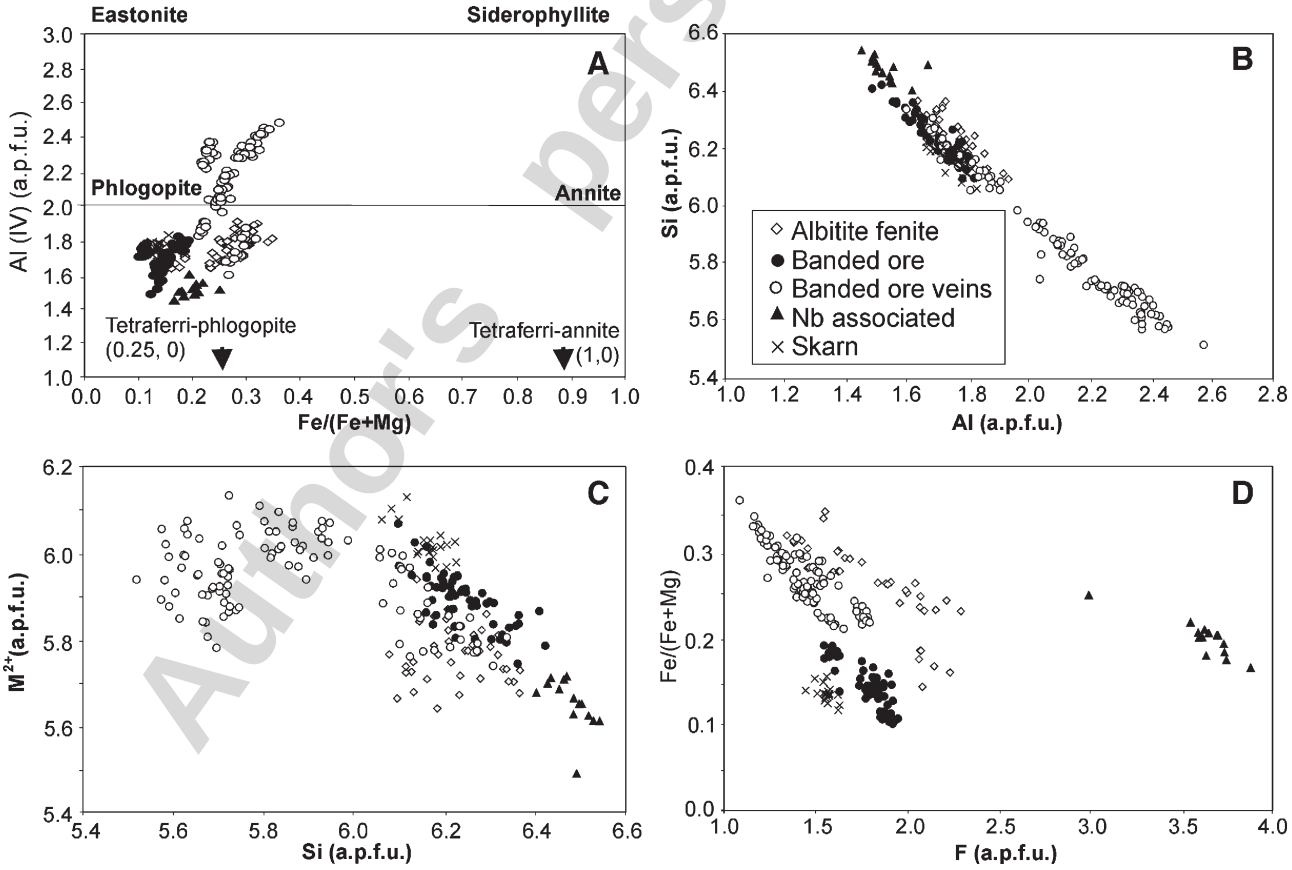


Fig. 7. Biotite chemistry from Bayan Obo. (A) Classification diagram (Deer et al., 1966), showing the non-ideal levels of Al on the tetrahedral site, and the co-ordinates for the composition of tetraferriphlogopite and tetraferriannite. (B)–(C) Bivariate plots of octahedral and tetrahedral site occupancy. M^{2+} = (Fe^{2+}+Mn+Mg). (D) Plot of Fe/(Fe+Mg) against fluorine showing the strong linear correlation, but at a range of slopes for different environments.

Author's personal copy

Table 4
Representative analyses of biotite from Bayan Obo

	Albitite fenite	Banded ores				Banded ore veins			Niobate assoc.	Skarn
	1995, P3 (30)	1995, P3 (13)	1995, P3 (17)	1995, P3 (29)	1996, P4 (6)	1995, P3 (18)	1995, P3 (18)	1995, P3 (7)	1999, P7 (67)	1999, P7 (82)
Na_2O	0.10	0.13	0.14	0.17	0.17	0.15	0.11	0.10	0.09	0.07
K_2O	9.92	10.54	10.59	10.63	10.57	9.88	10.04	10.18	10.71	10.84
CaO	0.01	0.04	0.16	0.12	0.15	0.07	0.06	0.00	0.06	0.00
MgO	19.30	23.42	23.10	24.20	21.62	18.69	18.45	18.06	20.78	23.51
BaO	n.a.[a]		0.01	0.03	0.03	2.32	0.13	0.25	n.a.#	
MnO	0.59	0.43	0.27	0.13	0.79	1.12	0.15	0.22	0.25	0.40
FeO	12.46	6.72	7.63	5.65	8.83	13.04	13.55	13.33	8.42	6.63
TiO_2	0.59	0.34	0.39	0.16	0.34	0.12	0.69	0.89	0.34	0.23
Al_2O_3	10.15	9.71	9.87	10.11	10.08	12.83	9.74	10.24	8.67	9.77
SiO_2	42.12	43.70	43.57	43.39	42.24	37.79	41.79	40.92	44.68	42.83
H_2O[b]	2.15	2.17	2.13	2.09	2.30	2.49	2.36	2.51	0.25	2.37
F	4.05	3.93	4.00	4.12	3.50	2.77	3.23	2.87	8.10	3.43
Cl	0.03	0.01	0.01	0.01	0.01	0.00	0.00	0.01	0.01	0.01
Total	101.46	101.14	101.88	100.80	100.64	101.26	100.29	99.58	102.37	100.09
O=F	1.71	1.65	1.69	1.74	1.47	1.17	1.36	1.21	3.41	1.45
O=Cl	0.01	0.00	0.00	0.00	0.00	0.00	0.00	0.00	0.00	0.00
Total	99.75	99.48	100.19	99.06	99.16	100.10	98.93	98.37	98.96	98.64
Formula calculated to 24 (O,OH,F)										
Na	0.029	0.037	0.039	0.047	0.047	0.044	0.031	0.029	0.025	0.020
K	1.866	1.935	1.937	1.951	1.975	1.905	1.911	1.953	1.997	2.011
Ca	0.001	0.006	0.024	0.018	0.024	0.011	0.010	0.000	0.010	0.000
Mg	4.267	5.050	4.969	5.218	4.745	4.233	4.127	4.073	4.554	5.126
Ba	0.000	0.000	0.001	0.001	0.002	0.138	0.007	0.015	0.000	0.000
Mn	0.073	0.053	0.033	0.015	0.098	0.143	0.019	0.028	0.031	0.049
Fe	1.530	0.805	0.912	0.677	1.077	1.641	1.684	1.671	1.026	0.803
Ti	0.065	0.037	0.042	0.018	0.037	0.013	0.077	0.101	0.037	0.025
Al	1.760	1.642	1.665	1.710	1.736	2.279	1.709	1.811	1.491	1.671
Si	6.207	6.282	6.246	6.236	6.182	5.707	6.232	6.152	6.529	6.225
OH[b]	2.108	2.21	2.185	2.13	2.381	2.679	2.481	2.637	0.26	2.422
F	1.886	1.78	1.813	1.87	1.618	1.321	1.519	1.361	3.74	1.576
Cl	0.006	0.00	0.002	0.00	0.001	0.000	0.000	0.002	0.00	0.002

[a] n.a. — not analysed.
[b] OH and H_2O calculated by difference assuming a full hydroxyl site occupancy.

Some of the A-site vacancy implied by the formula calculations (Table 4) may be also be accounted for by substitutions of the form $(Al^{3+}{}_{-1},K^{+}{}_{-1})$,$(Si^{4+}{}_{+1},\square_{+1})$. Biotites from some vein samples cutting the banded ores show Si and Al contents consistent with the phlogopite–eastonite solid solution (Monier and Robert, 1986).

The chloride content of all biotites is below the detection limits for the analytical conditions used (~ 0.03 wt.% Cl; ~ 0.06 wt.% F; 3σ). Fluoride contents (Fig. 7D) show consistent variations between sample types, alongside systematic correlations with crystal chemistry. Most significantly fluoride content shows a strong negative correlation with the Fe/(Fe+Mg) ratio (c.f. Rosenberg and Foit, 1977). Samples from banded ores and veins cutting banded ores show a relatively well defined linear relationship, with F contents ranging from ~ 1 to 2 atoms per formula unit (a.p.f.u.). Samples from albitite fenite are slightly F-enriched relative to this trend (F contents ranging from ~ 1.5 to 2.5 a.p.f.u.), and samples from the single niobate-bearing example show a very strong F-enrichment (F contents from 3 to 4 a.p.f.u.). Biotite from the Permian skarn sample is slightly F-depleted relative to other environments (Fig. 7D).

4.4. Amphibole chemistry

The results of analyses of amphibole chemistry are shown in Figs. 8 and 9, and summarised in Table 5. Discrimination and classification plots (Leake et al., 1997) indicate the majority of amphiboles from ore deposits and the carbonatite fenites to be either magnesioriebeckite or magnesioarfvedsonite (Fig. 8A, B). Only amphiboles

Author's personal copy

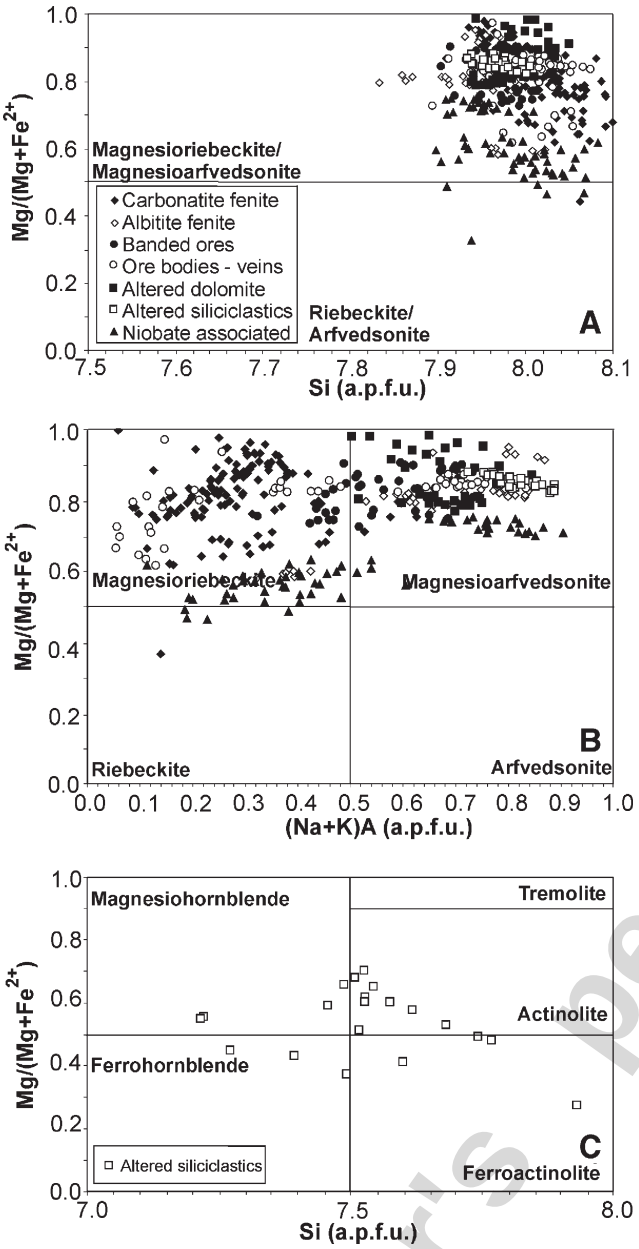


Fig. 8. Chemical classification of Bayan Obo amphiboles. Compositional limits from Leake et al. (1997).

from the slate sample from the east orebody show significantly different major element chemistry, and are classified as actinolite and hornblende (Fig. 8C). Compositional zonation is relatively limited within ore body amphiboles, with a maximum continuous increase of around 2 wt.% FeO from core to rim in one sample (1996, P4(7)) and little evidence of discrete growth zones. Zonation is more marked in fenite amphiboles (Fig. 4A), but with a relatively simple, non-oscillatory structure that probably represents change in the growth conditions with time rather than self-organisation (Yardley et al., 1991; Ortoleva et al., 1987).

The chlorine content of amphiboles is minimal, but all amphiboles contain significant fluoride. Fig. 9 shows bivariate plots for fluoride and other major element constituents of amphibole. For the plots shown fluorine shows positive correlations in individual sample types with magnesium on the octahedral site (Fig. 9A), and K and Ca on the alkali (A and B) sites (Fig. 9D, E), and negative correlations with Fe(III) on the octahedral site, and Si on the tetrahedral site (Fig. 9B, C). The total population of samples analysed do not define single linear trends, but show a series of separate trends with different slopes.

4.5. Apatite chemistry

The chemistry of apatites from Bayan Obo has previously been discussed in detail by Campbell and Henderson (1997). New data (Table 6) were acquired to supplement information on the evolution of halogen activities in the ore forming fluid and to attempt to use co-existing biotite and apatite for geothemometry (Zhu and Sverjensky, 1992). In all instances of co-existing biotite and apatite temperatures calculated are geologically unreasonable, with the majority of samples giving estimated temperatures in excess of 1000 °C, and never below 800 °C. This indicates that biotite and apatite are not in equilibrium within the banded ores. Apatite composition indicates halogen activities during the main banded ore forming events (apatite type II of Campbell and Henderson, 1997), and during vein formation (apatite III and IV of Campbell and Henderson, 1997). In terms of fluoride content, data from this study and from Campbell and Henderson (1997) indicate early apatite (Type I) has fluoride contents ranging from 3.26 to 3.86 wt.%, banded ore apatite (Type II) has fluoride contents from 2.78 to 4.17 wt.%, and vein apatite (Type III and IV) has fluoride contents from 2.13 to 3.91 wt.%.

5. Discussion

5.1. Mineralogical evolution of fenites and orebodies

The mineral assemblage developed at Bayan Obo must be considered as the product of a complex interaction of numerous metasomatic fluids and metamorphic events. To a first approximation the development of silicate mineral assemblages in the Bayan Obo fenites and ore bodies can be investigated in the system Na–Al–Fe–Si–O–H. Fig. 10 A and B show reactions in the system Na–Fe–Si–O–H in terms of temperature, the activity ratio a_{Na^+}/a_{H^+} and oxygen fugacity calculated using a version of SUPCRT92 (Johnson et al., 1992)

Author's personal copy

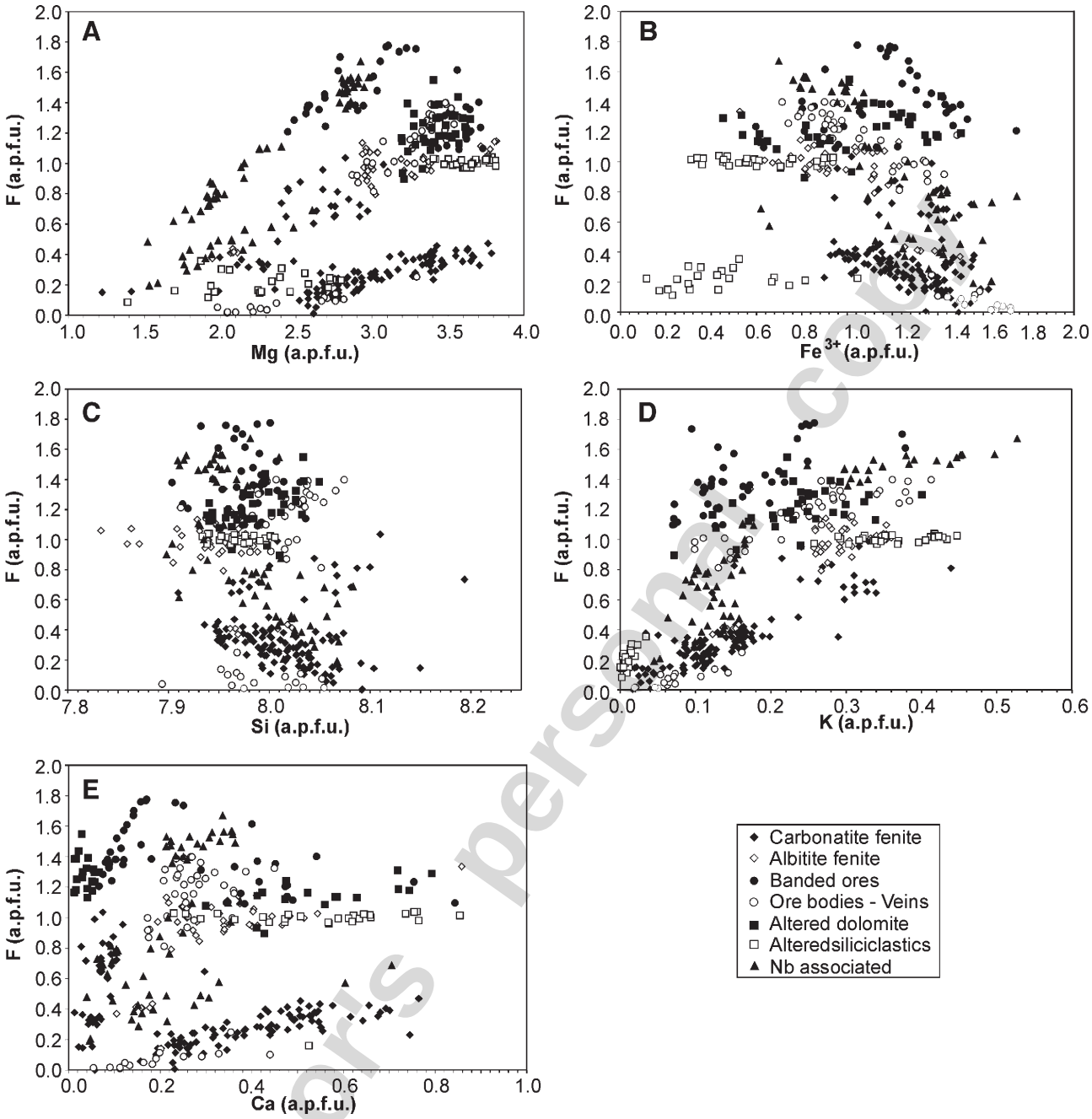


Fig. 9. Variation of fluorine content of Bayan Obo amphiboles with crystal chemistry. Note strong correlations with octahedral and A-site cations, and lack of correlation with tetrahedral site cations.

modified to include the heat capacity equation and internally consistent thermodynamic data for minerals of Holland and Powell (1990) by M. Reed. Full equations for all reactions are given by Miyano and Beukes (1997). Fig. 10A also illustrates the stability of albite relative to paragonite, and the effects of decreasing riebeckite activity. The primary effect of the magnesio-riebeckite substitution will be to expand the field of alkali amphibole stability at all temperatures, although no thermodynamic data exist for magnesio-end member alkali amphiboles which would allow this analysis to be extended. The shaded areas in both diagrams show the regions of aegirine and riebeckite-bearing assemblages for temperature ranges determined from fluid inclusions (Table 2; Smith et al., 2000). Temperatures for aegirine formation were determined directly from inclusions in aegirine crystals, whilst those for amphiboles are the temperature range of phase separation indicated by fluid inclusions in fluorite which is paragenetically related to the formation of blue amphibole in veins and banded ores (Smith and Henderson, 2000). Fig. 10C and D are constant temperature activity diagrams for the system

Author's personal copy

Table 5
Representative analyses of amphibole from Bayan Obo. Formulae calculated using the assumptions outlined in Leake et al. (1997)

	Carbonatite fenite		Albitite fenite		Banded ores		Banded ore veins		Altered dolomite		Altered siliciclastics		Niobate associated	
	1999, P7(96)	1999, P7(117)	1999, P7(103)	1995, P3(30)	1999, P3(16)	1996, P4(12)	1995, P3(18)	1996, P4(18)	1996, P4(7)	1996, P4(52)	1999, P7(127)	1999, P7(40)	1999, P7(67)	1996, P4(16)
Na_2O	8.15	6.17	7.12	7.46	8.11	7.10	6.80	7.73	7.08	8.80	6.16	0.69	6.99	6.95
K_2O	1.73	0.92	1.28	1.51	0.61	0.39	0.69	1.90	1.11	1.65	2.27	0.02	2.41	0.73
CaO	0.61	3.34	0.59	1.54	0.78	3.15	1.31	1.60	3.80	0.09	4.32	10.47	2.25	2.10
MgO	13.46	16.18	10.94	13.66	13.58	15.99	12.89	15.88	15.60	16.36	17.71	12.85	13.15	10.67
MnO	0.41	0.50	0.35	0.79	0.60	0.18	0.35	0.12	0.99	0.08	0.63	0.24	0.91	0.46
FeO	7.87	2.87	8.37	5.44	4.90	5.09	4.73	5.31	7.14	2.81	4.58	9.71	8.98	11.09
Fe_2O_3	8.94	11.09	13.06	11.40	13.57	8.45	14.81	8.38	5.65	11.06	5.55	9.62	7.40	10.81
Al_2O_3	0.82	0.34	0.83	1.27	0.13	0.26	0.59	0.16	0.51	0.27	0.28	2.40	0.51	0.57
SiO_2	57.25	56.52	55.23	54.69	55.90	56.82	55.76	56.91	55.80	57.95	56.09	51.91	53.91	54.70
TiO_2	0.30	0.04	0.12	0.06	0.03	0.10	0.04	0.00	0.06	0.11	0.06	0.17	0.14	0.09
Cl	0.02	0.00	0.00	0.00	0.02	0.01	0.01	0.01	0.01	0.03	0.00	0.00	0.00	0.02
F	1.71	0.65	1.06	2.14	3.00	2.55	0.31	2.96	2.52	3.16	2.27	0.50	3.36	1.25
H_2O[a]	1.29	1.82	1.57	1.07	0.68	0.91	1.96	0.71	0.90	0.65	1.04	1.83	0.45	1.45
Total	102.59	100.44	100.50	101.03	101.89	101.01	100.24	101.67	101.16	103.00	100.97	100.45	100.46	100.89
Cl=O	0.00	0.00	0.00	0.00	0.00	0.00	0.00	0.00	0.00	0.01	0.00	0.00	0.00	0.00
F=O	0.72	0.27	0.44	0.90	1.26	1.07	0.13	1.25	1.06	1.33	0.96	0.21	1.42	0.53
Total	101.86	100.16	100.06	100.13	100.62	99.93	100.11	100.43	100.10	101.67	100.01	100.24	99.05	100.36
Formulae to 24 (O,OH,F) following Leake et al. (1997)														
Na	2.223	1.681	1.996	2.074	2.237	1.944	1.877	2.120	1.961	2.365	1.692	0.194	1.995	1.962
K	0.311	0.165	0.236	0.276	0.111	0.071	0.125	0.344	0.203	0.292	0.412	0.004	0.454	0.135
Ca	0.093	0.504	0.091	0.238	0.119	0.477	0.201	0.243	0.582	0.013	0.658	1.627	0.355	0.328
Mg	2.845	3.417	2.376	2.944	2.904	3.392	2.757	3.375	3.347	3.409	3.773	2.794	2.909	2.334
Mn	0.049	0.060	0.042	0.096	0.072	0.022	0.042	0.014	0.119	0.009	0.076	0.030	0.114	0.056
Fe	0.924	0.337	1.010	0.651	0.581	0.600	0.562	0.627	0.852	0.326	0.542	1.173	1.104	1.347
FeIII	0.945	1.170	1.418	1.229	1.450	0.896	1.584	0.890	0.606	1.152	0.591	1.045	0.818	1.182
Al	0.135	0.056	0.141	0.215	0.021	0.043	0.099	0.027	0.085	0.043	0.047	0.409	0.088	0.098
Si	8.067	7.956	7.999	7.859	7.968	8.036	7.952	8.066	7.984	8.050	7.964	7.526	7.951	7.974
Ti	0.032	0.004	0.013	0.006	0.004	0.010	0.004	0.000	0.006	0.011	0.007	0.018	0.015	0.010
Cl	0.004	0.001	0.000	0.000	0.004	0.003	0.001	0.002	0.003	0.007	0.000	0.001	0.000	0.004
F	0.761	0.289	0.483	0.971	1.348	1.139	0.138	1.325	1.138	1.384	1.018	0.227	1.565	0.577
OH[a]	1.236	1.710	1.517	1.029	0.647	0.857	1.861	0.673	0.859	0.609	0.982	1.772	0.435	1.419

[a] OH and H_2O calculated by difference assuming a full hydroxyl site occupancy.

Na–Fe–Al–Si–O–H (Albino, 1995), constructed at 1 kbar pressure, with fO_2 buffered by hematite–magnetite equilibrium.

Aegirine and riebeckite co-exist stably within the carbonatite fenites at Bayan Obo. This assemblage is not unusual for fenites (e.g. Appleyard and Woolley, 1979; Currie et al., 1992; Andersen and Austrheim, 1991). Fig. 10A shows that the assemblage aegirine plus reibeckite plus magnetite is stable at high Na^+ activity (typically log $a_{Na^+}/a_{H^+}>6$). It could exist at lower a_{Na^+}/a_{H^+} in the presence of hematite. Within the orebodies aegirine is replaced by magnesio-arfvedsonite and magnesio-riebeckite which are also developed in dolomite and elsewhere in the banded ores. Using riebeckite as a proxy for these phases, Fig. 10A and B show that riebeckite is stable to lower Na activity, relative to assemblages containing aegirine, magnetite, and quartz. It is also stable to below fO_2 buffered by magnetite–hematite equilibrium relative to the same assemblage (log $fO_2>-39$ at 300 °C). For a_{Na^+}/a_{H^+} buffered by albite–paragonite equilibrium, quartz-free riebeckite-bearing assemblages are stable to ~ 375 °C and log $fO_2=-31$. This activity ratio is too low to represent the fluids at Bayan Obo, where albite is the stable phase in the orebodies and fenites. Fig. 10A indicates the minimum log a_{Na^+}/a_{H^+} for co-existing aegirine and riebeckite is around 6 at magnetite–hematite equilibrium. Increasing log a_{Na^+}/a_{H^+} to 6 increases these maximum stability limits to in excess of 700 °C, and indicates that riebeckite will be the stable phase for fluids with fO_2 buffered by hematite–magnetite equilibrium below ~ 575 °C (Fig. 10B). Aegirine plus magnetite are only stable at higher a_{Na^+}/a_{H^+} in the fluid. The shift from aegirine to riebeckite as the dominant alteration phase at Bayan Obo

Author's personal copy

Table 6
Representative analyses of apatites carried out for this study

	Banded ores				Banded ore veins		
	1995, P3(13)	1995, P3(17)	1995, P3(29)	1996, P4(6)	1996, P4(46)	1995, P3(7)	1995, P3(18)
Na_2O	0.38	0.35	0.20	0.28	0.21	0.27	0.40
CaO	55.11	55.21	56.14	56.18	55.14	54.38	53.48
MgO	0.00	0.01	0.00	0.00	0.01	0.00	0.01
SrO	0.30	0.21	0.15	0.15	1.34	0.68	1.13
BaO	0.05	0.04	0.02	0.02	0.04	0.02	0.04
MnO	0.26	0.12	0.02	0.08	0.17	0.05	0.03
FeO	0.36	0.26	0.15	0.24	0.14	0.18	0.24
Al_2O_3	0.01	0.00	0.00	0.01	0.02	0.00	0.01
Y_2O_3	b.d.[a]	0.06	0.10	0.12	0.11	0.13	0.17
La_2O_3	b.d.[a]	0.03	0.08	0.06	0.10	0.05	0.15
Ce_2O_3	0.29	0.40	0.24	0.31	0.41	0.54	0.82
Nd_2O_3	0.39	0.60	0.18	0.30	0.23	0.55	0.70
SiO_2	b.d.[a]	0.05	0.04	0.06	0.03	0.07	0.04
SO_2	0.32	0.20	0.10	0.21	0.01	0.03	0.02
P_2O_5	41.36	41.25	42.08	41.81	41.65	41.13	41.14
H_2O[b]	0.41	0.60	0.42	0.66	0.52	0.86	0.63
F	3.20	2.93	3.21	2.88	3.05	2.54	2.85
Cl	0.01	0.01	0.01	0.00	0.00	0.01	0.01
Total	102.45	102.30	103.16	103.39	103.17	101.47	101.86
O=F	1.35	1.23	1.35	1.21	1.28	1.07	1.20
O=Cl	0.00	0.00	0.00	0.00	0.00	0.00	0.00
Total	101.10	101.06	101.80	102.18	101.89	100.40	100.66
Formulae to 26 (O, OH, F)							
Na_2O	0.031	0.029	0.016	0.022	0.017	0.022	0.033
CaO	9.998	10.063	10.074	10.116	9.989	10.032	9.850
MgO	0.000	0.002	0.001	0.000	0.002	0.000	0.002
SrO	0.029	0.021	0.015	0.015	0.131	0.067	0.112
BaO	0.003	0.003	0.001	0.001	0.002	0.001	0.003
MnO	0.037	0.017	0.002	0.012	0.024	0.007	0.004
FeO	0.051	0.036	0.021	0.033	0.019	0.026	0.035
Al_2O_3	0.001	0.001	0.001	0.002	0.003	0.001	0.002
Y_2O_3	0.000	0.006	0.009	0.011	0.010	0.011	0.015
La_2O_3	0.000	0.002	0.005	0.004	0.006	0.003	0.010
Ce_2O_3	0.018	0.025	0.014	0.019	0.026	0.034	0.052
Nd_2O_3	0.024	0.036	0.011	0.018	0.014	0.034	0.043
SiO_2	0.000	0.008	0.007	0.010	0.005	0.012	0.008
SO_2	0.051	0.031	0.016	0.034	0.001	0.004	0.003
P_2O_5	5.918	5.930	5.956	5.937	5.952	5.985	5.977
F	1.709	1.571	1.699	1.528	1.626	1.380	1.545
Cl	0.002	0.002	0.002	0.001	0.000	0.003	0.002
OH[b]	0.288	0.427	0.299	0.471	0.374	0.617	0.452

[a] Below detection.
[b] OH and H_2O calculated by difference assuming full hydroxyl site occupancy.

was, therefore, promoted by a decrease in T (Fig. 10C and D), but also strongly influenced by a decrease in fO_2 and a_{Na^+}/a_{H^+}. The decrease in fO_2 could be a result of the ingress of cooler fluids, with the fO_2 buffered by the presence of hematite and magnetite as the ore bodies developed over time, or from the periodic influx of unbuffered, external fluid with fO_2 below that defined by hematite–magnetite equilibrium. The a_{Na^+}/a_{H^+} ratio is unlikely to be buffered by the mineral assemblage at Bayan Obo, and probably represents the changes in fluid chemistry indicated by fluid inclusions (Smith and Henderson, 2000; Table 2). The presence of CO_2 in the fluid at Bayan Obo would move the lower limit of riebeckite stability to lower Na^+ activities and oxygen fugacities (Miyano and Klein, 1983). The reaction of aegirine to reibeckite can also be facilitated by a decrease in $a_{SiO_2(aq)}$ (Fig. 10C and D).

The arguments above focus on riebeckite as a proxy for amphibole at Bayan Obo. The actual amphibole composition includes major components of arfvedsonite

Author's personal copy

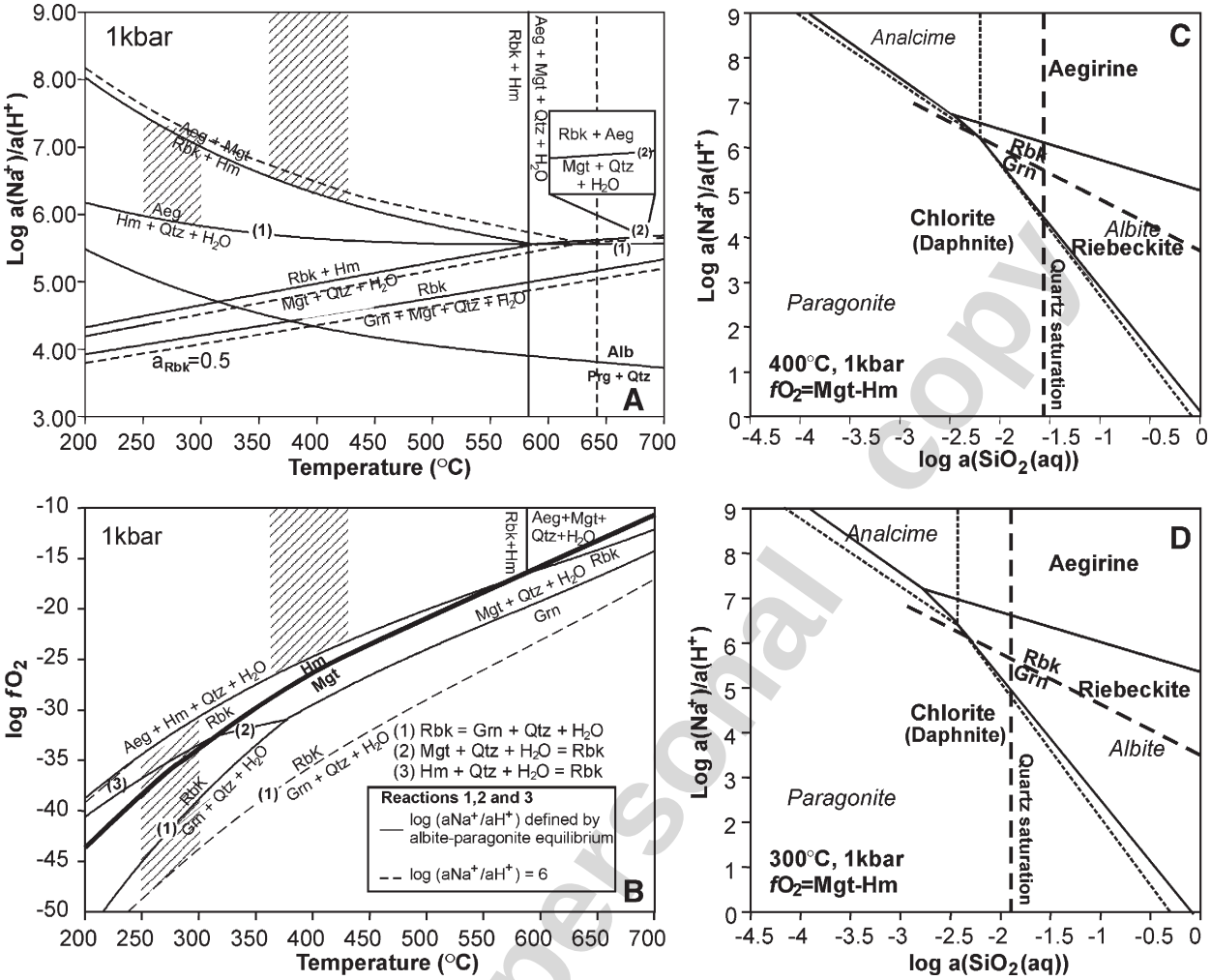


Fig. 10. Phase relations in the system Na–Fe–Si–O–OH. (A) Temperature–activity diagram at 1 kbar pressure. (B) Temperature–oxygen fugacity diagram at 1 kbar, with a_{Na^+}/a_{H^+} buffered by albite–paragonite equilibrium and at a fixed value of 5. Shaded areas in both diagrams show temperature range inferred from Bayan Obo fluid inclusions for aegirine and fluorite stage alteration. (C) and (D) a_{Na^+}/a_{H^+}–a_{SiO_2}(aq) at 1 kbar and 400 °C and 300 °C, with fO_2 buffered by hematite–magnetite equilibrium. Reactions given in full by Miyano and Beukes (1997). All diagrams are calculated for pure end-member compositions, except for the dashed line in (A), where $a_{riebeckite}=0.5$. See text for discussion.

and significant magnesium contents. Thermodynamic data are lacking for all these potential end members. Examination of simple model reaction stoichiometry (Eq. (1)) suggests that arfvedsonite occurrence implies lower fO_2 and higher a_{Na^+}/a_{H^+} than for riebeckite formation under the same P–T conditions.

$$\underset{\text{ARFVEDSONITE}}{4Na_3Fe^{II}_4Fe^{III}Si_8O_{22}(OH)_2} + 4H^+ + O_2 = \underset{\text{RIEBECKITE}}{4Na_2Fe^{II}_3Fe^{III}_2Si_8O_{22}(OH)_2} + 4Na^+ + 2H_2O \quad (1)$$

This analysis does not examine the influence of K^+ in the alteration process at Bayan Obo. The formation of biotite is the main manifestation of potassic alteration within the ores bodies, but within the overlying siliciclastic meta-sediments albitisation is overprinted by the formation of K-feldspar and hyalophane alongside biotite (Drew et al., 1990). Pollard (2001) attributed the shift in alteration from Na- to K-dominated in IOCG deposits to speciation changes in the fluid on aqueous-carbonic phase separation. Similar changes have also been attributed to cooling of the metasomatic system in fenites (Rubie and Gunther, 1983). Fluid inclusion data indicate both processes accompanied the introduction of more dilute fluids during the fluorite stage alteration with which biotite is associated.

5.2. Crystal chemistry and the halogen content of silicates

The relationship between the octahedral site occupancy and the halogen content of biotite is well known (e.g.

Author's personal copy

Rosenberg and Foit, 1977; Munoz, 1984). The composition of Bayan Obo biotite is consistent with this (Fig. 7D). An array of straight lines with differing slopes is shown on this plot, with clear differences between biotite from Permian skarns, the banded ores, the banded ore veins, the fenites and biotite associated with niobate mineralisation.

Previous studies have suggested that the F and Cl contents of amphiboles can be controlled by the *P–T* conditions and halogen activity in the co-existing fluid (e.g. Vanko, 1986), mineral structure and crystal chemistry (e.g. Morrison, 1991; Oberti et al., 1993; Sato et al., 1997). Oberti et al. (1993) showed that amphiboles have a strong preference for Fe^{2+}–Cl short-range order (resulting in Fe–F and Mg–Cl avoidance; Rosenberg and Foit, 1977), interactions between the O3′ anion site and K on the A site affect the halogen and hydroxyl chemistry, and that expansions and contractions of the lattice caused by halogen and hydroxyl substitutions are accommodated by expansion of the tetrahedral sheet by substitution of Al for Si. For crystal chemically controlled substitution of Cl for OH, the chlorine content of amphibole should therefore correlate positively with Fe^{2+}, K and Al IV. The fluoride ion is smaller than the hydoxyl ion, and so F substitution for OH should have no effect on the tetrahedral site, so for crystal chemically controlled substitution of F for OH, F should correlate positively with Mg^{2+} and K.

For the Bayan Obo amphiboles the plots given in Fig. 9 show positive correlations between F and Mg, K and Ca, and negative correlations of F with ferrous and ferric iron, and Si. In order to clarify the distinctions made between and within the paragenetic settings studied principle components analysis has been carried out on the entire amphibole data set. This technique is described in detail by Davis (2002), and has been previously applied to biotite and amphibole analyses by Kullerud (1995, 1996). Principle components analysis serves to reduce the number of variables in the data set by defining new variables that are linear combinations of the original variable set. The first new variable defines a vector in compositional space which is associated with the highest percentage variance of the original data set, the second is normal to the first, and is associated with next highest percentage variance, and so on. The principal components defined can be regarded as expressing complexly coupled exchange reactions responsible for the variation in mineral chemistry (Kullerud, 1995).

The results of this procedure are shown in Table 7 and plotted in Fig. 11. The first four eigenvectors identified account for 76% of the variance within the total population of amphibole analyses from Bayan Obo. The first principle component (PC1) expresses the major element variation on each crystallographic site within the amphiboles. PC2 emphasizes the covariation of the alkali site occupancy, Mg and F in varying amphibole chemistry. PC3 expresses the variation of Mg, Mn and Fe on the octahedral site. PC4 is largely weighted to the variation in Cl, which is close to its analytical detection limit, and so this component has less significance. The components clearly distinguish between the alkali amphiboles associated with the ore bodies and fenites,

Table 7
Results of principle components analysis of amphibole chemistry

		Component			
		1	2	3	4
Initial eigen values	Total	4.514	2.464	1.221	1.007
	% of variance	37.614	20.532	10.178	8.388
	Cumulative %	37.614	58.146	68.324	76.713
		Extracted components			
Variables	Na	0.871	−0.162	0.298	0.085
	K	0.564	0.618	0.242	0.035
	Ca	−0.829	0.458	−0.2	−0.071
	Mg	0.458	0.669	−0.562	0.061
	Mn	0.238	0.504	0.439	−0.067
	FeII	−0.668	−0.159	0.592	−0.13
	FeIII	0.327	−0.799	−0.034	0.079
	Al	−0.854	0.169	0.051	0.135
	Si	0.817	−0.321	−0.019	−0.136
	Ti	−0.496	0.014	0.245	0.158
	Cl	−0.006	−.05	0.026	0.947
	F	0.535	0.589	0.332	0.065

Author's personal copy

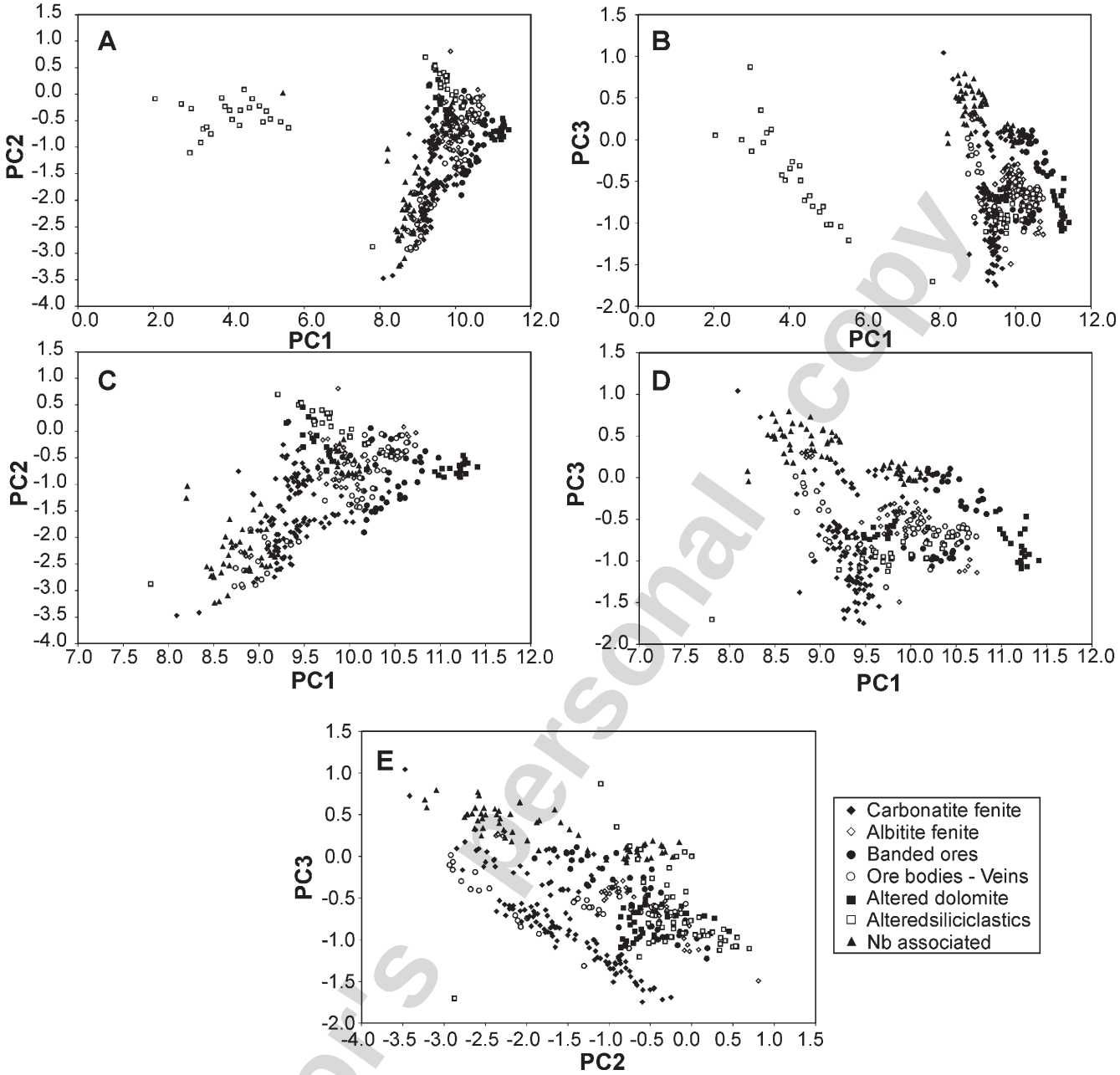


Fig. 11. Results of principle components analysis of Bayan Obo amphibole chemistry. Principle components are shown in Table 7.

Authors personal copy

and the hornblendic amphiboles hosted in the surrounding metasediments (Fig. 11 A and B). In Fig. 11 C and D the portions of these graphs showing the alkali amphiboles are plotted at a larger scale. Carbonatite fenite samples, and the albitite fenite sample all fall on different linear arrays, with groups of data from other textural settings within the ore bodies falling on each array. In particular niobate bearing samples all show high scores in PC3, corresponding to F-enriched amphiboles (Fig. 11E). The trends shown in this plot show the link between the hydroxyl site occupancy, the octahedral site and to a lesser extent the A-site cations with three main arrays of coupled substitutions at differing F-contents. A single linear array on a principal components plot would relate to a coupled substitution mechanism relative to an individual additive component (Kullerud, 1995). Multiple arrays mean that the range of amphibole compositions must be derived by coupled substitutions from a range of additive components. This strongly suggests that different phases of carbonatite or related magmatism at Bayan Obo, had differing fluid chemistries or formed under different *P–T* conditions. Fluids also infiltrated the orebodies under contrasting conditions, even within apparently comparable paragenetic stages. The close comparison between

fenite amphiboles of various types and the ore body amphiboles is consistent with a genetic link between fenitising and ore-forming fluids.

5.3. Fluid evolution trends in ore bodies and fenites

The relationship between biotite composition and the halogen chemistry of hydrothermal fluids has been the focus of detailed study, with a range of experimental studies (reviewed in Munoz, 1984) allowing the thermodynamic properties of end-member biotites to be estimated and mixing models to be proposed for biotite solid solutions (Zhu and Sverjensky, 1991, 1992). The relationship between biotite composition and fluid composition can be considered in terms of the reaction:

$$\begin{aligned}&\text{Annite}-\text{OH}_2+2\text{HF(aq)}\\&\quad=\text{Annite}-\text{F}_2+2\text{H}_2\text{O}\end{aligned}\qquad\text{(a)}$$

Assuming ideal mixing of Mg and Fe on the octahedral site, and OH and F on the hydroxyl site, but allowing for reciprocal mixing effects between the two sites, this reaction has the equilibrium constant:

$$K_{r(a)}=\frac{(\gamma_{\text{annite}-\text{F}_2}\cdot X_{\text{Fe}}^3\cdot X_{\text{F}}^2)\cdot a_{\text{H}_2\text{O}}^2}{(\gamma_{\text{annite}-\text{OH}_2}\cdot X_{\text{Fe}}^3\cdot X_{\text{OH}}^2)\cdot a_{HF}^2}$$

For which:

$$\log K_{r(a)}=\log\left(\frac{\gamma_{\text{annite}-\text{F}_2}}{\gamma_{\text{annite}-\text{OH}_2}}\right)+2\log\left(\frac{X_{\text{F}}}{X_{\text{OH}}}\right)+2\log\left(\frac{a_{\text{H}_2\text{O}}}{a_{\text{HF}}}\right)$$

The activity co-efficient ratio can be evaluated using the reciprocal solid solution model of Wood and Nicholls (1978) as shown by Zhu and Sverjensky (1992):

$$\ln\left(\frac{\gamma_{\text{annite}-\text{F}_2}}{\gamma_{\text{annite}-\text{OH}_2}}\right)=\frac{X_{\text{Mg}}\Delta G^o_{r(b)}}{RT}$$

Where $\Delta G^{\text{o}}_{r(b)}$ refers to the Gibbs free energy of the ion exchange reaction (b):

$$\begin{aligned}&\text{Annite}-\text{F}_2+\text{Phlogopite}-\text{OH}_2\\&\quad=\text{Annite}-\text{OH}_2+\text{Phlogopite}-\text{F}_2\end{aligned}\qquad\text{(b)}$$

This allows the following expression for the activity ratio of water and HF in equilibrium with biotite to be derived:

$$\log\left(\frac{a_{\text{H}_2\text{O}}}{a_{\text{HF}}}\right)=-\frac{1}{2}\frac{X_{\text{Mg}}\Delta G^o_{r(b)}}{2.303RT}-\log\left(\frac{X_{\text{F}}}{X_{\text{OH}}}\right)-\frac{1}{2}\frac{\Delta G^o_{r(a)}}{2.303RT}$$

With the simplifying assumption that octahedral Al (representing the siderophyllite and eastonite components) and Fe^{3+} have an equivalent effect on substitutions to Fe^{2+} (Zhu and Sverjensky, 1992), this equation predicts that for constant temperature the composition of biotite in equilibrium with a fluid with constant $a_{\text{HF}}/a_{\text{H}_2\text{O}}$ ratio, should plot as a straight line on a plot of Log $X_{\text{F}}/X_{\text{OH}}$ against X_{Mg}. Fig. 12A shows such a plot for biotite from the Bayan Obo ore bodies and carbonatite and albitite fenites. Contours of activity ratio were calculated using data for water from Kestin et al. (1984), for HF(aq) from the SUPCRT92 data base (Johnson et al., 1992), and for HCl(aq) from Sverjensky et al. (1991) using the web-enabled thermodynamic database of Bastrakov et al. (2004). Mineral properties at elevated temperature were calculated using the data of Zhu and Sverjensky (1991, 1992) for halogen bearing end members, and that of Berman (1988, 1990) for hydroxyl end members, and the entropy convention of Helgeson et al. (1978). All data used are internally consistent, and fluid properties are internally consistent with those used for the construction of activity diagrams in the system Na–Fe–Si–O–H. The mineral properties used in the two procedures are not fully internally consistent.

At 300 °C and 1 kbar biotites from banded ore veins indicate a log $a_{\text{HF}}/a_{\text{H}_2\text{O}}$ ratio of ~ −3.77, whilst biotites from the banded ores themselves, indicate a slightly lower ratio (~ −3.84). This is consistent with the buffering of the fluid within the banded ores to slightly lower HF activities than that in the veins by water–rock interaction and formation of fluorite and F-bearing silicates. The biotites from the albitite fenite plot slightly higher than this suggesting either that they formed from a fluid of higher a_{HF} or at a slightly lower temperature, distinguishing the fluids involved in fenitisation from the fluid interacting with the orebodies. Biotites associated with niobate mineralisation have F contents significantly higher than those seen for either the rest of the orebodies, or the fenites. This can only be explained by niobate mineralisation at temperatures up to 100 °C lower than in the main ore forming stages, or by the involvement of a significantly more F-rich fluid in niobate mineralisation, with log $a_{\text{HF}}/a_{\text{H}_2\text{O}}$ values near to −2.62. The second possibility is more likely, as there is little evidence for biotite formation and niobate mineralisation at significantly lower temperature than those inferred for primary fluorite mineralisation.

Similar calculations for the compositions of apatites from the banded ore and vein stages for apatite compositions of 1.47–1.63 a.p.f.u. and 1.09–1.97 a.p.f.u. respectively are shown in Fig. 12B. Banded ore apatites indicate consistently lower $a_{\text{HF}}/a_{\text{H}_2\text{O}}$ than biotite, and

Author's personal copy

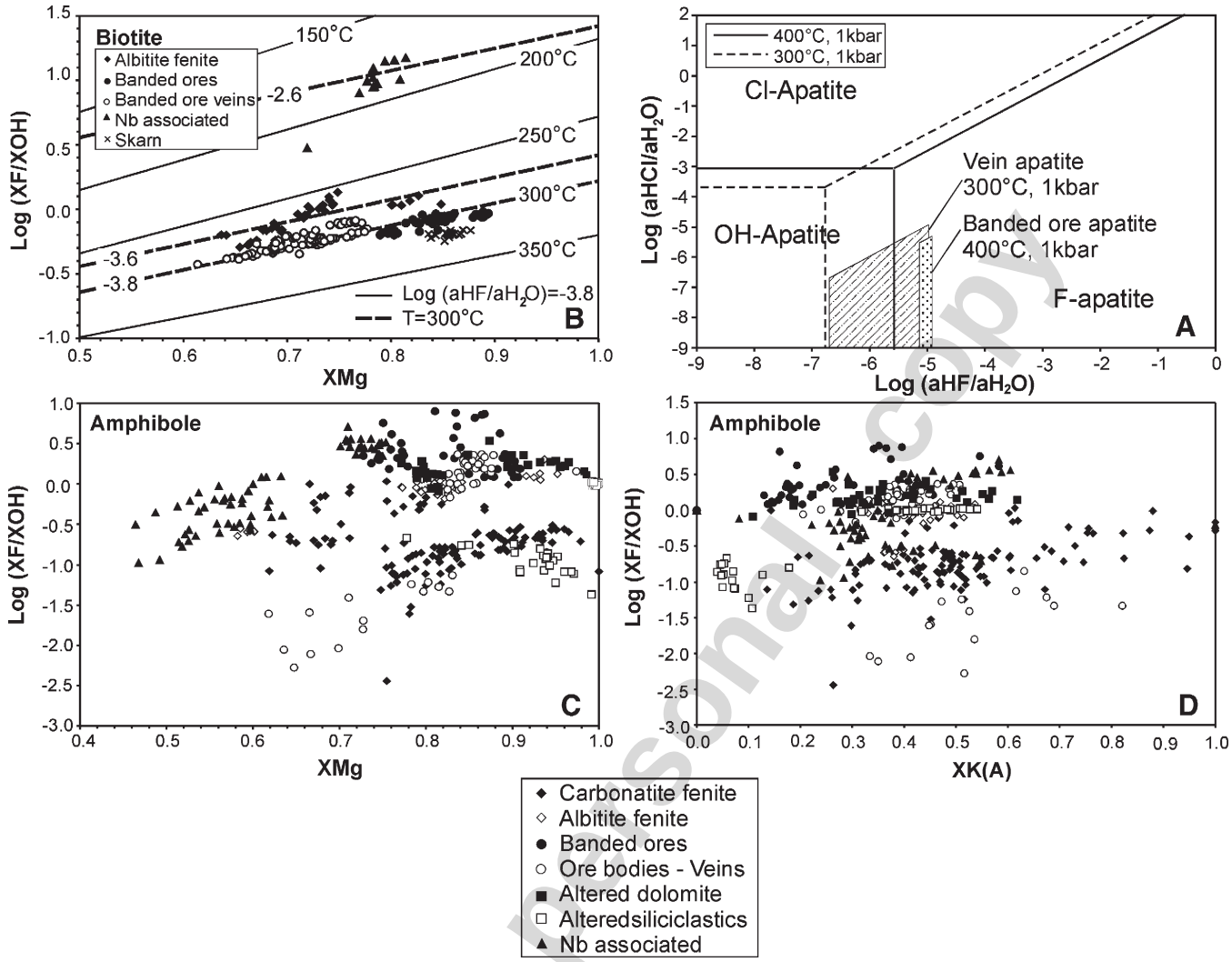


Fig. 12. Interpretation of hydrothermal fluorine chemistry at Bayan Obo. (A) Log (X_F/X_{OH}) vs. X_{Mg} plot for Bayan Obo biotites. Contours show equilibrium fluid compositions at 1 kbar for the conditions shown. Both diagrams calculated using the data of Zhu and Sverjensky (1991, 1992) and other data source listed in the text. (B) Species predominance diagram for apatite at 1 kbar and 400–300 °C. Solid and dashed lines show the fluid composition for equal mole fractions of species. Shaded boxes show conditions limited by the composition of banded ore and vein apatite. (C) and (D) Plots of amphibole chemistry in terms of Log (X_F/X_{OH}), X_{Mg} and X_K on the alkali site. See text for discussion.

reflect a different stage in the paragenesis linked to slightly more dilute fluids (Table 2). Vein apatite also indicates lower a_{HF}/a_{H_2O} than co-existing biotite. Pure fluor-apatites do occur at Bayan Obo (Campbell and Henderson, 1997) and place an upper limit on the levels of a_{HF} that can be differentiated using apatite chemistry. These may, therefore, be consistent with the compositions indicate by biotite chemistry.

Comparable thermodynamic data do not exist for fluorine end-member amphiboles, but consideration of the crystal chemical controls on fluorine substitution into amphiboles, and the correlations presented above, suggests that similar relationships to those for biotite may be plotted for amphibole, albeit complicated by the affects on the hydroxyl site from the alkali site, as well as the octahedral site. Plots of the mole fraction of Mg and K against the log X_F/X_{OH} should distinguish amphiboles formed from different fluid or under different conditions in the same way as for biotite. These variables strongly reflect principle components 2 and 3 identified above (Table 7). In Fig. 12C a linear array is formed by the niobate associated samples, and one banded ore sample, a second array at lower X_F is formed by altered dolomite samples, the remaining banded ore samples, one carbonatite fenite sample, the albite fenite and some vein samples, and a third is defined by the remaining carbonatite sample, and the remaining vein samples. The metasedimentary samples show distinct trends. The difference in vein samples reflects different vein mineralogies, with the low X_F sample being from an aegirine

Author's personal copy

vein sample, and the two higher X_F samples from apatite–fluorite vein fill post-aegirine in one vein, and from an apatite–fluorite vein in the other.

Amphibole and biotite chemistry at Bayan Obo reflect repeated cycles of mineralisation, and metasomatism associated with the introduction of differing fluids even within an apparently consistent paragenetic stage. Some of the differences in chemistry may also be linked to subsequent phases of metamorphism, although there is little evidence for re-equilibration of biotite or amphibole with lower salinity fluids (c.f. Dilles, 1987). The niobate mineralisation is the paragenetically latest stage of high field strength element mineralisation at Bayan Obo, excepting the remobilisation of the rare earths and formation of Ba–REE minerals associated with barite and sulphide deposition (Smith et al., 2000). The composition of co-existing amphiboles clearly indicates much higher HF activities at this stage, indicating the introduction of a new batch of fluorine-rich fluid. The level of HF activity does not correspond to that indicated by of the analysed fenites. Niobium transport in hydrothermal solutions has not been extensively studied, but its understanding has major implications for the formation of Nb deposits, and for the formation of phases potentially useful in geochronology. The evidence from this study indicates that F may be key in the formation of hydrothermal niobate mineralization (Gagnon et al., 2004), and in controlling the magmatic mineralogy of Nb (Mitchell and Kjarsgaard, 2004).

If a reasonable estimate of water activity can be made, and the speciation of F under the conditions of interest is known the calculated a_{HF}/a_{H_2O} ratio can be used to estimate the F content of the hydrothermal fluid. Zhu and Sverjensky (1991) showed that for fluid in equilibrium with fluorite in the system $MgO–SiO_2–CaF_2–H_2O$ F speciation was dominated by HF° down to 400 °C and 1 kbar. Simple calculations of fluid speciation at 300 °C and water-saturated vapour pressure in an 8 wt.% NaCl solution with pH buffered by the presence of gaseous CO_2, the concentrations of Ca and F fixed by saturation with calcite and fluorite, and fO_2 buffered by hematite–magnetite equilibrium carried out using PHREEQC 2.8 (Parkhurst and Appelo, 1999) show HF(aq) accounting for ~ 44% of the F species in solution, with the majority of the remainder being accounted for by F^-, NaF°, and CaF^+. For reasonable conditions for the fluorite stage fluid at Bayan Obo (8 wt.% salinity; $X_{CO_2}=0.12$, 300 °C, 1 kbar) the water activity for the system $NaCl–H_2O–CO_2$ calculated from the equation of state of Bowers and Helgeson (1983) using the FLUIDS package of Bakker (2003) is ~ 1.38, consistent with experimental constraints at ~ 1 kbar and 300 °C (Shmulovich and Graham, 1996). As a neutral aqueous species, HF has an activity coefficient of one. Applying these approximations to the activity ratios calculated from biotite chemistry would indicate approximately ~ 9–12 ppm F in the fluid for the fluorite stage of the banded ores and veins, but up to 140 ppm for fluids associated with niobate mineralisation. The niobium mineralisation must in this case be the result of the influx of an externally derived fluid with notably higher F contents than those that had already interacted with the ore bodies. Niobate mineralization at higher temperatures than those of fluorite alteration would require even higher a_{HF} in the fluid. These calculations are sensitive to variations in F-speciation with pH and other variables in fluid composition, but provide an initial estimate of the F-contents of the hydrothermal fluids. The low values in fluorite stage fluids are probably due to the buffering of the F-content by fluoritisation of calcite and dolomite.

Comparisons with previous data are hampered by the variable use of fugacity and activity ratios in the literature, but a fugacity ratio based on the thermodynamic data of Zhu and Sverjensky (1991, 1992) can be calculated using the equations of Munoz (1992). The fluid compositions of banded ore, vein hosted and fenite biotites are within ranges previously calculated for fluids in equilibrium with late stage granitoid biotites (e.g. Coulson et al., 2001; Selby and Nesbitt, 2000). The biotites associated with niobate minerals in this instance are at the high end of this range, but within the range of fluid compositions indicated for carbonatites and early post-magmatic fluids in the Fen complex, Norway (Andersen and Austrheim, 1991), and for fluorite-bearing syenite-associated fluids in Dronning Maud Land, Antarctica (Markl and Piazolo, 1998). Estimates of actual F contents of hydrothermal fluids are still relatively low, however, compared to analyses of fluid inclusion leachates from high temperature veins in granitoids in S.W. England which in some cases contained over 1000 ppm F (Bottrell and Yardley, 1988; Smith et al., 1996).

5.4. Implications for the genesis of the Bayan Obo ore bodies

Previous $^{40}Ar–^{39}Ar$ data have been used to suggest that the amphiboles of Bayan Obo area were formed in specific settings at widely different times, with the formation of fenite amphiboles, metamorphic amphibole in siliciclastics and dolomite marble, and ore body amphibole being temporally distinct (Chao et al., 1997). $^{40}Ar–^{39}Ar$ ages for metasomatic amphibole at Bayan Obo range from 1260 Ma to 343 ± 3 Ma. Chao et al.

Author's personal copy

(1997) assigned these dates to metamorphic amphibole, variable hydrothermal vein hosted amphiboles (including both the oldest and youngest examples), and amphibole formed during deformation of the host dolomite in the period 800–900 Ma. In each case the ages calculated were assumed to represent minimum formation ages. In such a case it would be expected that each generation of amphiboles should be chemically distinct. However, Wartho (1995) showed chemical re-equilibration of amphibole from Bayan Obo during at least one post-formation reheating event, leading to false isochron ages ranging from 1198±81 Ma to 697±36 Ma derived from a single sample. Much of the range of ages inferred from Bayan Obo amphiboles may therefore be the result of an extensive post-formation thermal history.

The data presented here show that composition cannot be used to completely distinguish amphiboles from distinct paragenetic settings, but that amphiboles from each setting show common features between fenites, dolomite marble and ore bodies, although there are different clusters in chemical variables associated with different fenites. This suggests that, despite the prolonged, multistage fluid evolution history at Bayan Obo, a fenite signature can still be identified in the ore bodies, strongly supporting the interpretation of the involvement of carbonatite magmatism with ore genesis, with different phases of dyke formation introducing fluids of contrasting chemistry. The chemistry of silicates at Bayan Obo is consistent with multiple events of fluid infiltration, at least some of which had characteristics in common with the fenitising fluids associated with carbonatites.

6. Conclusions

The evolution of the silicate alteration mineralogy at Bayan Obo is consistent with fluid evolution trends indicated by fluid inclusion microthermometry. Early, Na-rich, oxidised fluids were responsible for the formation of aegirine and aegirine–augite alongside magnetite and REE minerals. The shift to magnesio-riebeckite and magnesio-arfvedsonite as the dominant silicate alteration minerals was driven by a fall in temperature from 400–450 °C to less than 300 °C and may have been accompanied by the martisation of magnetite. Although falling temperature would be sufficient to drive such reactions, they are also promoted by decreasing Na^+ activity, possibly as a result of the ingress of more dilute fluids, and by decreasing oxygen fugacity buffered by the assemblage magnetite+hematite at Bayan Obo.

The fluorine contents of amphibole and biotite are highly variable throughout the deposits. Linear trends in the variation of F with other compositional variations indicate at least three phases of metasomatism during amphibole and biotite formation, with indicated halogen activities falling on the same linear trends as those from the ore bodies. This strongly suggests the involvement of carbonatite derived fluids in the formation of the ore bodies, with different fluids arising from different phases of carbonatite dyke formation. Although REE-mobility has been demonstrated throughout the geological evolution of the Bayan Obo ore bodies, only the most F-rich fluids produced significant niobate mineralisation. Comparison with experimental evidence indicates that such high F activities may be critical for the formation of niobium mineralisation.

The data presented here re-inforce previous interpretations that the Bayan Obo ores are the product of prolonged, multistage processes. However, the chemistry of amphiboles in both ore bodies and fenites show much in common, and support models for the genesis of the Bayan Obo ores involving carbonatite-related fluids interacting with dolomite marble at some stages of ore genesis, and subsequent metamorphism of the resulting ore bodies to give the range of radioisotope ages derived for the area.

Author's personal copy

Acknowledgements

Thanks to John Spratt and Terry Williams for assistance and advice on SEM and electron microprobe analyses. Constructive comments from two anonymous referees also helped improve this manuscript.

References

Albino, G.V., 1995. Sodium metasomatism along the Melones fault zone, Sierra Nevada Foothills, California, USA. Mineralogical Magazine 59, 383–399.

Andersen, T., Austrheim, H., 1991. Temperature–HF fugacity trends during crystallisation of calcite carbonatite magma in the Fen complex, Norway. Mineralogical Magazine 55, 81–94.

Appleyard, E.C., Woolley, A.R., 1979. Fenitization: an example of the problems of characterizing mass transfer and volume changes. Chemical Geology 26, 1–15.

Bai, G., Yuan, Z., 1985. Carbonatites and Related Mineral Resources. Geological Publishing House, pp. 107–140 (In Chinese).

Bakker, R.J., 2003. Package FLUIDS 1. Computer programs for analysis of fluid inclusion data and for modelling bulk fluid properties. Chemical Geology 194, 3–23.

Bastrakov, E., Shvarov, Y., Girvan, S., Cleverley, J., Wyborn, L., 2004. FreeGs: web-enabled thermodynamic database for modelling of geochemical processes. In: McPhie, J., McGoldrick, P. (Eds.), Dynamic Earth: Past, Present and Future. Abstracts of the 17th Australian Geological Convention. Hobart, Tasmania, Australia, p. 52.

Berman, R.G., 1988. Internally consistent thermodynamic data from minerals in the system Na_2O–K_2O–CaO–MgO–FeO–Fe_2O_3–Al_2O_3–SiO_2–TiO_2–H_2O–CO_2: representation, estimation and high temperature extrapolation. Journal of Petrology 29, 445–522.

Berman, R.G., 1990. Mixing properties of Ca–Mg–Fe–Mn garnets. American Mineralogist 75, 328–344.

Bottrell, S.H., Yardley, B.W.D., 1988. The composition of a primary granite-derived ore fluid from S.W. England, determined by fluid inclusion analysis. Geochimica et Cosmochimica Acta 52, 585–588.

Bowers, T.S., Helgeson, H.C., 1983. Calculation of the thermodynamic and geochemical consequences of non-ideal mixing in the system H_2O–CO_2–NaCl on phase-relations in geologic system: Equation for H_2O–CO_2–NaCl fluids at high pressuresand temperatures. Geochimica et Cosmochimica Acta 47, 1247–1275.

Brod, J.A., Gaspara, J.C., de Araujo, D.P., Gibson, S.A., Thompson, R.N., Junqueira-Brod, T.C., 2001. Phlogopite and tetra-ferriphlogopite from Brazilian carbonatite complexes: petrogenetic constraints and implications for mineral-chemistry systematics. Journal of Asian Earth Sciences 19, 265–296.

Campbell, L.S., Henderson, P., 1997. Apatite paragenesis in the Bayan Obo REE–Nb–Fe ore deposit, Inner Mongolia, China. Lithos 42, 89–103.

Campbell, L.S., Compston, W., Sircombe, K., 2000. ^{232}Th–^{208}Pb (SHRIMP) Dates of Zircons From the Bayan Obo REE–Nb–Fe Deposit, China. Mantle Materials, Processes and Products, With VMSG and MDSG RIP Sessions. Abstract Volume.

Chao, E.C.T., Back, J.M., Minkin, J.A., Ren, Y., 1992. Host-rock controlled epigenetic, hydrothermal metasomatic origin of the Bayan Obo REE–Fe–Nb ore deposit, Inner Mongolia, P.R.C. Applied Geochemistry 7, 443–458.

Chao, E.C.T., Tatsumoto, M., Back, J.M., Minkin, J.A., McKee, E.H., Ren, Y., 1993. Multiple lines of evidence for establishing the mineral paragenetic sequence of the Bayan Obo rare earth ore deposit of Inner Mongolia, China. In: Maurice, Y.T. (Ed.), Proceedings of the International Association on the Geology of Ore Deposits, 8th Symposium volume, pp. 53–73.

Chao, E.C.T., Back, J.M., Minkin, J.A., Tatsumoto, M., Wang, J., Conrad, J.E., McKee, E.H., Zonglin, Hou, Qingrun, Meng, Shengguan, Huang, 1997. The Sedimentary Carbonate-Hosted Giant Bayan Obo Ree–Fe–Nb Ore Deposit of Inner Mongolia, China: a Corner Stone Example for Giant Polymetallic Ore Deposits of Hydrothermal Origin. USGS Bulletin, vol. 2143. 65 pp.

Coulson, I.M., Dipple, G.M., Raudsepp, M., 2001. Evolution of HF and HCl activity in magmatic volatiles of the gold-mineralized Emerald Lake pluton, Yukon Territory, Canada. Mineralium Deposita 36, 594–606.

Currie, K.L., Knutson, J., Temby, P.A., 1992. The Mud Tank carbonatite complex, central Australia — an example of metasomatism at mid-crustal levels. Contributions to Mineralogy and Petrology 109, 326–339.

Davis, J.C., 2002. Statistics and Data Analysis in Geology, Third edition. John Wiley and Sons, New York. 638 pp.

Deer, W.A., Howie, R.A., Zussman, J., 1966. An introduction to the rock forming minerals. Longman Scientific and Technical. 528 pp.

Dilles, J.H., 1987. Petrology of the Yerington Batholith, Nevada: evidence for evolution of porphyry copper ore fluids. Economic Geology 71, 772–794.

Drew, L.J., Meng, Q., Sun, W., 1990. The Bayan Obo iron-rare earth–niobium deposits, Inner Mongolia, China. Lithos 26, 46–65.

Gagnon, J.R., Samson, I.M., Fryer, B.J., Williams-Jones, A.E., 2004. The composition and origin of hydrothermal fluids in a NYF-type granitic pegmatite, South Platte District, Colorado: evidence from LA-ICP-MS analysis of fluorite and quartz-hosted fluid inclusions. Canadian Mineralogist 42, 1331–1355.

Helgeson, H.C., Delany, J.M., Nesbitt, H.W., Bird, D.K., 1978. Summary and critique of the thermodynamic properties of the rock-forming minerals. American Journal of Science 278-A.

Hitzman, M.W., Oreskes, N., Einaudi, M.T., 1992. Geological characteristics and tectonic setting of Proterozoic iron oxide (Cu–U–Au–REE) deposits. Precambrian Research 58, 241–287.

Holland, T.J.B., Powell, R., 1990. An enlarged and internally consistent thermodynamic data set with uncertainties and correlations: the system K_2O–Na_2O–CaO–MgO–MnO–FeO–Al_2O_3–TiO_2–SiO_2–C–H_2–O_2. Journal of Metamorphic Geology 8, 89-24.

Hou, Z., 1989. The Bayan Obo Fe–Nb–REE deposit: its basic geological features, metallogenesis and genetic model. Geology and Prospecting 25 (7), 1–5 (In Chinese).

Johnson, J.W., Oelkers, E.H., Helgeson, H.C., 1992. SUPCRT92: a software package for calculating the standard molal thermodynamic properties of minerals, gases, aqueous species and reactions from 1 to 5000 bars and 0 to 1000 °C. Computers in Geoscience 18, 899–947.

Kestin, J., Sengers, J.V., Kamgar-Parsi, B., Levelt-Sengers, J.M.H., 1984. Thermophysical properties of fluid H_2O. Journal of Physical and Chemical Reference Data 13, 175–183.

Kullerud, K., 1995. Chlorine, titanium and barium-rich biotites: factors controlling biotite composition and the implications for garnet–biotite geothermometry. Contributions to Mineralogy and Petrology 120, 42–59.

Kullerud, K., 1996. Chlorine-rich amphiboles: interplay between amphibole composition and an evolving fluid. European Journal of Mineralogy 8, 355–370.

Le Bas, M.J., Keller, J., Tao, K., Wall, F., Williams, C.T., Zhang, Z., 1992. Carbonatite dykes at Bayan Obo, Inner Mongolia, China. Mineralogy and Petrology 46, 195–228.

Le Bas, M.J., Spiro, B., Yang, X., 1997. Oxygen, carbon and strontium isotope study of the carbonatitic dolomite host of the Bayan Obo Fe–Nb–REE deposit, Inner Mongolia, N. China. Mineralogical Magazine 61, 531–541.

Leake, B.E., 21 members of the IMA CNMMN Subcommittee: Nomenclature of Amphiboles, 1997. Report of the Subcommittee on Amphiboles of the International Mineralogical Association Commission on New Minerals and Mineral Names. Mineralogical Magazine 61, 295–321.

Liu, Y.L., Yang, G., Chen, J.F., Du, A.D., Xie, Z., 2004. Re–Os dating of pyrite from giant Bayan Obo REE–Nb–Fe deposit. Chinese Science Bulletin 49, 2627–2631.

Markl, G., Piazolo, S., 1998. Halogen-bearing mineral in syenites and high-grade marbles of Dronning Maud Land, Antarctica: monitors of fluid compositional changes during late-magmatic fluid–rock interaction processes. Contributions to Mineralogy and Petrology 132, 246–268.

Meng, Q., 1982. The genesis of the host rock dolomite of Bayan Obo iron deposits and the analysis of its sedimentary environment. Geological Reviews 28, 481–489 (In Chinese with English Abstract).

Mitchell, R.H., Kjarsgaard, B.A., 2004. Solubility of niobium in the system $CaCO_3$–CaF_2–$NaNbO_3$ at 0.1 GPa pressure: implications for the crystallization of pyrochlore from carbonatite magma. Contributions to Mineralogy and Petrology 148, 281–287.

Miyano, T., Klein, C., 1983. Conditions of riebeckite formation in the iron-formation of the Dales Gorge Member, Hamersly Group, Western Australia. American Mineralogist 68, 517–529.

Miyano, T., Beukes, N.J., 1997. Mineralogy and petrology of the contact metamorphosed amphibole asbestos-bearing Penge iron formation, Eastern Transvaal, South Africa. Journal of Petrology 38, 651–676.

Author's personal copy

Monier, G., Robert, J.L., 1986. Muscovite solid solutions in the system K_2O–MgO–FeO–Al_2O_3–SiO_2–H_2O: an experimental study at 2 kbar P_{H2O} and comparison with natural Li-free white micas. Mineralogical Magazine 50, 257–266.

Morrison, J., 1991. Compositional constraints on the incorporation of Cl into amphiboles. American Mineralogist 76, 1920–1930.

Munoz, J.L., 1984. F–OH and Cl–OH exchange in micas with applications to hydrothermal ore deposits. In: Bailey, S.W. (Ed.), Micas. Reviews in Mineralogy, vol. 13, pp. 469–493.

Munoz, J.L., 1992. Calculation of HF and HCl fugacities from biotite compositions: revised equations. Geological Society of America, Abstracts with Programs 24, A221.

Oberti, R., Ungaretti, L., Cannillo, E., Hawthorne, F.C., 1993. The mechanism of Cl incorporation in amphibole. American Mineralogist 78, 746–752.

Ortoleva, P., Merino, E., Moore, C., Chaldam, J., 1987. Geochemical self –organisation. 1. Reaction-transport feedbacks and modelling approach. American Journal of Science 287, 979–1007.

Parkhurst, D.L., Appelo, C.A.J., 1999. User's guide to PHREEQC (Version 2) – a computer program for speciation, batch-reaction, one dimensional transport, and inverse geochemical calculations. US Geological Survey Water-Resources Investigations Report 99-4259.

Pollard, P.J., 2001. Sodic(–calcic) alteration in Fe-oxide–Cu–Au districts: an origin via unmixing of magmatic H_2O–CO_2–NaCl±$CaCl_2$–KCl fluids. Mineralium Deposita 36, 93–100.

Ren, J., 1985. A brief account on the geology of rare earth mineralization in China. In: Xu, G., Xiao, J. (Eds.), New Frontiers in Rare Earth Science and Applications, vol. 1. Science Press, Beijing, pp. 39–41.

Ren, Y., Zhan, Y., Zhan, Z., 1994. Study on the heat events of ore-forming Bayan Obo deposit. Acta Geoscientia Sinica 1–2, 95–101.

Rosenberg, P.E., Foit Jr., F.F., 1977. Fe^{2+}–F avoidance in silicates. Geochimica et Cosmochimica Acta 41, 345–346.

Rubie, D.C., Gunther, W.D., 1983. The role of speciation in alkaline igneous fluids during fenite metasomatism. Contributions to Mineralogy and Petrology 82, 165–175.

Sato, H., Yasmaguchi, Y., Makino, K., 1997. Cl incorporation into successively zoned amphiboles from the Ramnes Cauldron, Norway. American Mineralogist 82, 316–324.

Selby, D., Nesbitt, B.E., 2000. Chemical composition of biotite from the Casino porphyry Cu–Au–Mo mineralization, Yukon, Canada: evaluation of magmatic and hydrothermal fluid chemistry. Chemical Geology 171, 77–93.

Shmulovich, K.I., Graham, C.M., 1996. Melting of albite and dehydration of brucite in H_2O–NaCl fluids to 9 kbars and 700–900 °C: implications for partial melting and water activities during high pressure metamorphism. Contributions to Mineralogy and Petrology 124, 370–382.

Smith, M.P., Henderson, P., 2000. Preliminary fluid inclusion constraints on mineralising fluid evolution in the Bayan Obo Fe–REE–Nb deposit, Inner Mongolia, China. Economic Geology 95, 1371–1388.

Smith, M.P., Wu, C., 2000. The geology and genesis of the Bayan Obo Fe–REE–Nb deposit: a review. In: Porter, T.M. (Ed.), Hydrothermal Iron Oxide Copper–Gold and Related Deposits: a Global Perspective. Australian Mineral Foundation, Adelaide, pp. 271–281.

Smith, M.P., Banks, D.A., Yardley, B.W.D., Boyce, A., 1996. Fluid inclusion and stable isotope constraints on the genesis of the Cligga Head Sn–W deposit, S.W. England. European Journal of Mineralogy 8, 961–974.

Smith, M.P., Henderson, P., Campbell, L.S., 2000. Fractionation of the REE during hydrothermal processes: constraints from the Bayan Obo Fe–REE–Nb deposit, Inner Mongolia, China. Geochimica et Cosmochimica Acta 64, 3141–3160.

Sverjensky, D.A., Hemley, J.J., D'Angelo, W.M.D., 1991. Thermodynamic assessment of hydrothermal alkali feldspar–mica–aluminosilicate equilibria. Geochimica et Cosmochimica Acta 55, 989–1004.

Tao, K., Yang, Z., Zhang, Z., Wang, W., 1998. Systematic geological investigation on carbonatite dykes in Bayan Obo, Inner Mongolia, China. Scientia Geologica Sinica 33, 73–83 (In Chinese with English abstract).

Vanko, D.A., 1986. High-chlorine amphiboles from oceanic rocks: product of highly-saline hydrothermal fluids? American Mineralogist 71, 51–59.

Wang, Z., 1973. The genetic features of the REE-Fe ore deposit related to sedimentation–metamorphism–hydrothermal metasomatism. Geochimica 1, 5–11.

Wang, J., Tatsumoto, M., Li, X., Premo, W.R., Chao, E.C.T., 1994. A precise ^{232}Th–^{208}Pb chronology of fine grained monazite: age of the Bayan Obo REE–Fe–Nb ore deposit, China. Geochimica et Cosmochimica Acta 58, 3155–3169.

Wartho, J., 1995. Apparent argon diffusive loss $^{40}Ar/^{39}Ar$ age spectra in amphiboles. Earth and Planetary Science Letters 134, 393–407.

Wood, B.J., Nicholls, J., 1978. The thermodynamic properties of reciprocal solid solutions. Contributions to Mineralogy and Petrology 66, 389–400.

Wu, C., Yuan, Z., Bai, G., 1996. Rare earth deposits in China. In: Jones, A.P., Wall, F., Williams, C.T. (Eds.), Rare Earth Minerals: Chemistry, Origin and Ore Deposits. Chapman and Hall, pp. 281–310.

Yardley, B.W.D., Rochelle, C.A., Barnicoat, A.C., Lloyd, G.E., 1991. Oscillatory zoning in metamorphic minerals: an indicator of infiltration metasomatism. Mineralogical Magazine 55, 357–365.

Yuan, Z., Bai, G., Wu, C., Zhang, Z., Ye, X., 1992. Geological features and genesis of the Bayan Obo REE ore deposit, Inner Mongolia, China. Applied Geochemistry 7, 429–442.

Zhang, P., Zhang, R., Yang, Z., 1994. Mineralogical and petrological studies on carbonatite dukes in Bayan Obo, Nei Mongol, China, and their implications to rare earth mineralisation. Journal of Rare Earths 12, 300–302.

Zhu, C., Sverjensky, D.A., 1991. Partitioning of F–Cl–OH between minerals and hydrothermal fluids. Geochimica et Cosmochimica Acta 55, 1837–1858.

Zhu, C., Sverjensky, D.A., 1992. F–Cl–OH partitioning between biotite and apatite. Geochimica et Cosmochimica Acta 56, 3435–3467.

Author's personal copy